Regional Studies in Marine Science 35 (2020) 101131

Contents lists available at ScienceDirect

Regional Studies in Marine Science

journal homepage: www.elsevier.com/locate/rsma

# Wind and tide effects on the Choctawhatchee Bay plume and implications for surface transport at Destin Inlet

R. Cyriac [a,b,*], J.C. Dietrich [a], C.A. Blain [c], C.N. Dawson [d], K.M. Dresback [f], A. Fathi [d,e], M.V. Bilskie [g], H.C. Graber [i], S.C. Hagen [g,h], R.L. Kolar [f]

[a] *Department of Civil, Construction, and Environmental Engineering, North Carolina State University, Campus Box 7908, 2501 Stinson Drive, Raleigh, NC, 27695, United States of America*
[b] *Atkins, 1616 E Milbrook Street, Raleigh, NC, 27609, United States of America*
[c] *Oceanography Division, Naval Research Laboratory, Stennis Space Center, MS, 39529, United States of America*
[d] *Oden Institute for Computational Engineering and Sciences, The University of Texas at Austin, Austin, TX 78712, United States of America*
[e] *ExxonMobil Research and Engineering, Corporate Strategic Research, 1545 Route 22 East, Annandale, NJ 08801, United States of America*
[f] *School of Civil Engineering and Environmental Science, University of Oklahoma, 202 W Boyd Street, Norman, OK, 73019, United States of America*
[g] *Center for Coastal Resiliency, Louisiana State University, 124 C Sea Grant Hall, Baton Rouge, LA, 70803, United States of America*
[h] *Department of Civil and Environmental Engineering, Louisiana State University, 3255 Patrick F Taylor Hall, Baton Rouge, LA, 70803, United States of America*
[i] *Department of Ocean Sciences, Rosenstiel School of Marine and Atmospheric Sciences, University of Miami, 4600 Rickenbacker Causeway, Miami, FL, 33149, United States of America*

A R T I C L E   I N F O

*Article history:*
Received 2 January 2019
Received in revised form 26 January 2020
Accepted 30 January 2020
Available online 7 February 2020

*Keywords:*
ADCIRC
Plume dynamics
Cold fronts
Florida Panhandle
SCOPE
CARTHE

A B S T R A C T

Multiple river-dominated estuaries line the northern Gulf coast and introduce substantial density variations. Their plumes have been shown to be highly sensitive to wind and tide effects, but in studies with limited observations and idealized wind forcing. This study explores these effects with a dynamic model that can represent the full behavior from river through estuary to shelf, and for a period with extensive observations. The inner shelf adjacent to Choctawhatchee Bay, a micro tidal estuary situated along the Florida Panhandle, is subject to buoyant, brackish outflows during the ebb-phase of the tidal cycle.

In December 2013, experiments were performed in this region to study mechanisms that influence near-shore surface transport. Satellite imagery showed a visible brackish surface plume at Destin during low tide. The goal of the present study is to quantify variability in the plume signature due to changes in tidal and wind forcing. Density-driven flows near Destin Inlet are modeled with the recently-enhanced, three-dimensional, baroclinic capabilities of the ADvanced CIRCulation (ADCIRC) model. Modeled tides, salinities and plume signature are validated against in-situ observations and satellite imagery. Model results reveal substantial changes in the length, width and orientation of the plume as the wind direction varied on consecutive days due to winter cold fronts. During a period of near-constant winds and variability in tidal amplitude, the model predicted a larger plume during spring tides than during neap conditions. Coriolis effects on the plume are minimized due to its small scale nature. Therefore, when the wind forcing is weak, the plume signature spreads radially from the inlet with slight preference to the down-shelf. The Choctawhatchee Bay plume is representative of other small-scale plumes formed in river-dominated and micro-tidal environments, and this work demonstrates the sensitivity of these plumes to changing environmental conditions.



## 1. Introduction

Freshwater inflows from riverine sources interact with the coastal ocean in the vicinity of estuarine mouths. These river plumes can create strong density gradients near the coastline that can cause the slowing down and convergence of offshore surface material (Roth et al., 2017) and thus prevent its transport toward the shoreline. The interaction of these outflows with the shelf waters also determine the fate and transport of river-borne nutrients, sediments, larvae, plankton, etc. (Mestres et al., 2007; Xia et al., 2007; Chant et al., 2008; Shi et al., 2010; Androulidakis and Kourafalou, 2011; Greer et al., 2018). Therefore, river plumes play an important role in regulating the biogeochemical processes occurring at the shelf, and knowledge of plume behavior and

* Corresponding author at: Atkins, 1616 E Milbrook Street, Raleigh, NC, 27609, United States of America.
*E-mail address:* rcyriac@ncsu.edu (R. Cyriac).

https://doi.org/10.1016/j.rsma.2020.101131

the key factors that govern it is important for local coastal and estuarine resource management.

Factors that influence plume behavior can be grouped into two categories: (a) those related to the geometry of the coastline, which include the width of the river mouths and the alignment of the coastline; and (b) the external forcing conditions, which include tides, river discharge, prevailing winds, currents, etc. Idealized plumes in the absence of any external forcing are expected to form a re-circulating bulge at the river mouth and spread down-shelf in the direction of Kelvin wave propagation due to effects of the earth's rotation. The shape of the bulge and the amount of freshwater transported in the down-shelf current are dependent on the width of the river mouths and the plume outflow velocity, which can be quantified using the Rossby number. Discharges from narrow river mouths are accompanied by high outflow velocities and therefore have a high Rossby number. Such plumes are expected to have a larger offshore spreading, and freshwater transport in the down-shelf direction is less prominent. Estuaries with wider river mouths are typically associated with lower Rossby numbers due to their relatively low velocities and they experience the effects of rotation more prominently with a recirculating bulge and down-shelf freshwater transport. The presence of realistic forcings such as ambient currents and prevailing winds can distort this behavior by enhancing or restricting the growth of the recirculating bulge and down-shelf current (Choi and Wilkin, 2007; Garvine, 1995; Fong and Geyer, 2002; Jurisa and Chant, 2012; Falcieri et al., 2013).

The dominant role played by local wind forcing in the spreading of surface advected plumes across the continental shelf is documented in several observational (e.g. Janzen and Wong, 2002; Whitney and Garvine, 2005; Osadchiev and Sedakov, 2019) and modeling (e.g. Xing and Davies, 1999; Fong and Geyer, 2001; Choi and Wilkin, 2007) studies. During light winds, plumes are more affected by the effects of rotation and exhibit a preferential down-shelf movement. Downwelling winds tend to increase this alongshore transport, whereas upwelling winds increase the offshore spreading of the plumes. Offshore winds are expected to increase the offshore spread, whereas onshore winds restrict the plume to the coastline. In addition to the direction, the wind magnitude is also important and the Wedderburn number can be computed to identify critical wind speeds at which wind effects begin to dominate buoyancy effects (Jurisa and Chant, 2012; Dzwonkowski et al., 2015; Zhao et al., 2018).

Brackish plumes generated by high-discharge river systems with wide mouths have been the subject of numerous observational and numerical studies (e.g., Johnson et al., 2001; Guo and Valle-Levinson, 2007; Chant et al., 2008; Ou et al., 2009; Pan et al., 2014; Tarya et al., 2015; Yu et al., 2018). However, only limited studies have analyzed the response of small-scale river plumes, whose impacts are more localized and whose features are distinct from those of larger plumes but also share similarities. The Mzymta river plume formed off the northeastern shore of the Black Sea is an example of a small scale plume. Satellite observations indicated that unlike large plumes, the Mzymta plume did not form a recirculating bulge even under low wind conditions but was transported offshore. Onshore winds caused an upstream (up-shelf) accumulation of the river plume whereas offshore and downwelling winds were accompanied by down-shelf freshwater transport and upwelling winds resulted in offshore spreading of the plume (Osadchiev and Sedakov, 2019). Another small river plume influenced by wind forcing is the Wanquan River plume located in Hainan, a tropical island in China. Model results based on nearly uniform wind conditions indicate that downwelling favorable winds favor down-shelf plume spreading and upwelling and offshore winds transport the plume offshore, whereas onshore winds transport water in the up-shelf direction (Zhao et al., 2018). Typically, small scale plumes are also shallow and surface advected and tend to respond rapidly to wind forcing. This behavior is illustrated by the response of the Maipo River Plume located in central Chile to diurnal variability in the local sea breeze. When wind forcing is weak, Coriolis effects dominate and the plume is confined near the inlet and tending to turn in the down-shelf direction. However, as the onshore sea breeze begins and the wind speeds increased, the direction of plume spreading was reversed and it starts to flow in the up-shelf direction (Pinones et al., 2005). The Berau river plume located in the Indonesian archipelago is an example of a small plumes in near equatorial regions where the Coriolis force is nearly zero. Plume spreading was observed to be primarily in the windward direction in this region (Tarya et al., 2015).

Small scale plumes are also formed at the mouths of several bays and estuaries in the Northern Gulf of Mexico (NGOM). These river-dominated estuaries have limited connectivity to the NGOM and form shallow plumes that introduce cross-shore salinity and velocity gradients in the shelf waters and form density fronts where surface material converges or slows (Roth et al., 2017). During an oil spill, which are frequent in the these estuarine plumes have the potential to act as natural barriers that prevent oil from beaching against the coastline (Roth et al., 2017). Therefore, the ability to predict the plume behavior at the mouth of these estuaries is crucial for planning oil spill response operations in the Gulf.

The buoyant plume from Mobile Bay, Alabama, a river-dominated estuarine system with a narrow and shallow connection to the shelf, has been studied via satellite imagery and in-situ observations (Stumpf et al., 1993; Dzwonkowski et al., 2015). The plume was found to be sensitive to wind forcing despite relatively low wind speeds. The shallow nature of the plume made it highly susceptible to wind forcing, with the wind becoming more effective in modifying the plume structure, via weakening of the density gradients as the plume expanded offshore. Downwelling winds caused a westward elongation of the surface-advected plume, and upwelling winds reversed and widened the plume. Perdido Bay estuary, situated adjacent to Mobile Bay along the Florida-Alabama coast, is another semi-enclosed bay system that interacts with the coastal ocean through a narrow inlet. Model salinities forced by spatially uniform and idealized wind conditions show that the plume is farthest offshore for northerly winds and confined closest to the coast and smallest for southerly winds. Like the Mobile Bay plume, the Perdido Bay plume was predicted to extend westward for easterly downwelling-favorable winds and is deflected offshore and eastward for westerly upwelling-favorable winds. In the absence of wind forcing, the plume has a relatively large size that spreads offshore and along the coast in both directions (Xia et al., 2011).

Although small scale plumes are less intense and their impacts are localized, their behavior has significant implications for the sustenance of local ecosystems. Additionally, though broad similarities exist across small plumes in their behavior, there are subtle differences in their characteristics depending on the freshwater input, coastline alignment, local wind patterns, outflow angle etc. Therefore, there is merit in understanding the unique spatial and temporal scales associated with plume behavior at each study site, and this is a significant motivation for this work. The focus of the present study is the behavior of the small-scale river plume from Choctawhatchee Bay, the third largest estuary in Florida. The bay which is located to the east of Mobile Bay and Perdido Bay and is representative of other Gulf of Mexico estuaries, supports a rich and diverse ecosystem and provides great economic benefit to the adjacent coastal communities through fisheries, navigation and recreational activities. The bay connects to the Gulf of Mexico via the narrow Destin Tidal Inlet. The coastline adjacent to Destin is vulnerable to the impacts of offshore oil spills. During the aftermath of the Deepwater Horizon oil spill in 2010, oil washed up against the beaches in this area. The ability to forecast the nearshore surface transport of offshore chemical and biological material can enhance the efficiency of oil spill response and fisheries management operations, which are important concerns for coastal communities around Choctawhatchee Bay. This requires a sound knowledge of the spatial and temporal gradients in the surface transport in the inner continental shelf, which are primarily determined by the behavior of the ebb-phase plume.

The few existing studies that investigate inner shelf salinity transport near Destin are based on the Surfzone Coastal Oil Pathways Experiments (SCOPE), which were conducted in December 2013 (Fig. 1). The aims of these experiments, which consisted of drifter deployments, dye releases, ADCP and CTD measurements, were to better understand the processes that are important for the transport of surface material. Along-shore velocities measured offshore of Santa Rosa Beach, which is located roughly 7 km west of Destin Inlet, describe the wind- and plume-driven nature of the surface currents in the inner shelf (Roth et al., 2017). Drifters were released at Destin during the tidal ebb-phase to study plume behavior. Moderate winds with an easterly component were observed to create a coastal jet, which formed a coastal barrier that prevented offshore drifters from beaching. Surface currents, during light and variable winds, were also observed to prevent drifter transport to the beach.

The present study builds on above findings from SCOPE and aims to further expand our understanding of the Choctawhatchee Bay plume. Although field measurements provide important insights about the wind- and plume-driven surface currents in the vicinity of Destin, key questions still remain about the spatial and temporal scales associated with plume behavior. Variability in the surface plume geometry on consecutive days of variable wind and tidal forcing is still unknown. What is the length and width of the ebb-phase plume that exits out of Destin Inlet? Does the plume geometry exhibit substantial changes as passing cold fronts bring about changes in wind direction in consecutive days? What are the magnitudes of these changes? What is the plume response in the absence of wind forcing? By answering these questions, this study aims to bridge the gaps in our understanding of plume behavior at Destin and thereby provide insights that would be useful for predicting nearshore surface transport pathways in the vicinity of Destin and similar estuarine systems.

To answer the above questions, we adopt a numerical modeling approach. Typically, most plume modeling studies rely on numerical experiments with idealized uniform winds applied over a few days to evaluate plume response to differences in wind direction and magnitude. In reality, however, coastal environments might be subject to rapidly varying wind patterns with shorter time scales such as in the case of winter cold fronts (typical in the Florida Panhandle) that can cause a 360 degree reversal in wind direction over the course of 2–3 days. In the present study we apply realistic winds that capture this variability in a three-dimensional, baroclinic, unstructured-mesh, estuarine- and shelf-scale model to investigate the plume response on consecutive days of variable tidal and wind forcing. Changing wind conditions and spring–neap variability in tidal conditions are expected to cause significant differences in the plume response on consecutive days. We first validate model predictions against in-situ salinity observations, satellite imagery, and drifter pathways. The validated model is then applied to quantify the length and width of the plume signature (geometry of the river plume as described by the surface salinity contours) on consecutive days of near-constant tides and variable wind directions, and on consecutive days of near-constant wind speeds and neap-to-spring variability in the tidal forcing. This study is novel in two ways. As mentioned previously, very few studies have investigated the dynamics of the wind- and plume-driven circulation offshore of Choctawhatchee Bay, and this study is a unique modeling effort that contributes to the scientific understanding of the characteristics of the Choctawhatchee River Plume. Secondly, this is the first time a recently-enhanced, three-dimensional, baroclinic version of the ADvanced CIRCulation (ADCIRC) model (Luettich et al., 1992; Westerink et al., 2008; Fathi et al., 2019), which has been widely applied for depth-averaged tidal and storm surge studies (Bunya et al., 2010; Dietrich et al., 2012; Passeri et al., 2015; Bilskie et al., 2016; Cyriac et al., 2018), is applied to represent density-driven estuarine and shelf circulation.

## 2. SCOPE observations near the Choctawhatchee Bay system

The study area is located in the estuarine and shelf waters in the vicinity of Choctawhatchee Bay, which is aligned in an east–west direction along the Florida Panhandle. Numerous bayous and creeks lining its banks are sources of freshwater for the bay. However, the bay receives 90% of its freshwater input from the Choctawhatchee River (CR) (Handley et al., 2007), which enters the bay at its eastern end. The bay is about 43 km long and has an average width of about 5 km with depths ranging from 3 to 10 m. It opens into the NGOM via the East Pass or Destin Inlet, which is about 450 m wide. The inlet contains a channel with depths varying from above 10 m at the estuarine end to around 4 m in the inlet region to about 7 m at the eastern end, where the inlet connects to the Gulf of Mexico (Valle-Levinson et al., 2015; Handley et al., 2007). The West Florida continental shelf is a broad, low energy area, with the 50 m isobath located at a distance of 30 km from the mouth of Choctawhatchee Bay. Tides are diurnal and weak in this region (Murphy and Valle-Levinson, 2008; Bilskie et al., 2016) with spring and neap tidal ranges of 0.5 m and 0.15 m respectively (Huguenard et al., 2016).

A series of experiments, collectively referred to as the Surfzone Coastal Oil Pathways Experiments (SCOPE, http://carthe.org/scope/), were conducted in this region by scientists from the Consortium for Advanced Research on Transport of Hydrocarbon in the Environment (CARTHE, http://carthe.org/). Field observations were collected during SCOPE to identify processes that influence surface transport in the inner shelf, which need to be better understood to improve future predictions of nearshore oil transport pathways in the event of an oil spill. During a 3-week period between 3–17 December 2013, data were collected with GPS-equipped surface drifters, helicopters, drones, balloons/kites, jet skis, small boats, ADCPs, CTD casts, and dye releases to describe nearshore wave and current movements (Valle-Levinson et al., 2015; Huguenard et al., 2016; Roth, 2016; Roth et al., 2017). Observations collected during SCOPE provide insights into the wind- and plume-driven nature of the inner shelf circulation offshore of Destin Inlet during specific dates/times during the experiment.

SCOPE observations confirm that tides near Destin Inlet are diurnal and similar to those observed at the NOAA gage at Panama City Beach. In the middle of Choctawhatchee Bay, tidal amplitudes were attenuated to 30% of the amplitudes at the entrance, and with a phase delay of 5.5 h (Valle-Levinson et al., 2015). During spring tides, observations indicate a moderate brackish outflow from Choctawhatchee Bay, which spreads radially outward in a semi-elliptical manner with an along-shore extent of about 3.5 km and a cross-shore extent of about 7.0 km. Plume velocity was opposed to the ambient currents to the west of the inlet, creating a distinct convergence zone that was visible in satellite imagery (Huguenard et al., 2016).

Cold fronts associated with extratropical storms are common during winter in the NGOM. These fronts propagate from west to east over 3 to 10 day periods and cause a 360 degree reversal

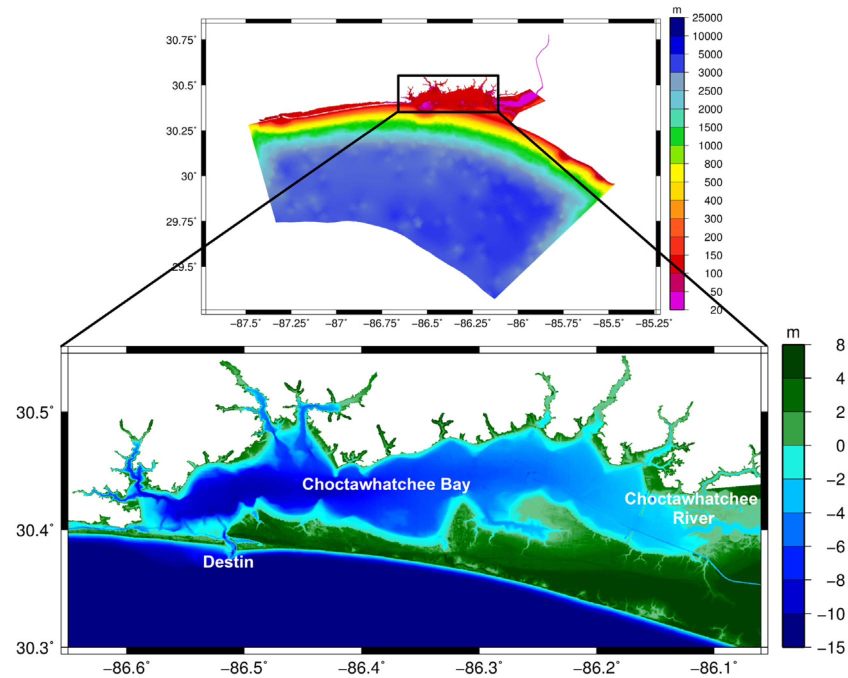


**Fig. 1.** Unstructured ADCIRC mesh used in the present study. Top panel shows contours of element spacing. Bottom panel shows the bathymetry and topography values (m) in and near the Choctawhatchee Bay.

in wind direction, with winds shifting from being southwesterly pre-front to northwesterly post-front (Roth, 2016; Feng and Li, 2010). During December 2013, several cold fronts lasting between 3 to 5 days passed over the study area with average wind speeds of 5 m/s. These cold fronts cause rapid along-shore current reversals in the inner shelf with westward flow slowing from about 0.2 m/s to zero within an hour and accelerating to about 0.2 m/s eastward within 1 to 2 days (Roth, 2016).

Drifters were released within the inlet during the ebb stage to identify the orientation of the Choctawhatchee River Plume as it emerges into the inner shelf. During easterly winds, the plume forms a coastal jet that flows west, parallel to the beach, and acts as a barrier that prevents surface drifters from beaching. During weak and variable winds, the plume expands radially outward without any preferential movement toward the east or the west. In both cases, plume boundaries introduce horizontal velocity gradients that cause drifters deployed outside the plume to converge along plume edges or be redirected offshore (Roth et al., 2017). Thus, offshore plume boundaries are expected to act as natural barriers that prevent surface material such as oil from beaching. When onshore winds carry oil to the shore, the plume can be effective near the inlet in reducing the amount of oil that washes ashore during the ebb stages (Kuitenbrouwer et al., 2018). The efficiency of these barriers depends on the interaction of these plume fronts with the ambient shelf currents (Roth, 2016).

The largest waves recorded during the experiment period had a significant wave height of about 0.5 m and coincided with the passage of a cold front that occurred between 12–16 December. Throughout the experiment, relatively larger waves occurred when winds were from the south ahead of the frontal passage. Wave heights were reduced when winds were from any other direction due to limited fetch (Roth, 2016). Discharge from the Choctawhatchee River during SCOPE was about 150 $m^3/s$, which is close to its annual minimum.

SCOPE datasets have provided rich insights into several aspects of the shelf circulation near Choctawhatchee Bay. However, due to the limitations associated with a field experiment, the characteristics of the ebb-phase plume have only been observed at specific instances during that two-week period in December 2013. The relative impacts of wind and tidal forcing on the Choctawhatchee River Plume is still unknown. Variability in plume geometry due to changes in the realistic wind speeds and changes in tidal amplitudes brought about by spring and neap tides have not been investigated previously.

Numerical models provide a greater flexibility to analyze the response of the coastal ocean to variability in the environmental forcing conditions. The aim of the present study is to develop a three-dimensional, numerical model for the Choctawhatchee Bay and Destin Inlet system that is validated against salinity profiles, satellite imagery and drifter movements collected during SCOPE. The validated model is then applied to quantify the plume signature and its variability in response to changing tidal and wind forcing. Model results quantify variability in the surface plume geometry of the Choctawhatchee Bay plume, and the predicted trends can be applied to investigate plume response to cold fronts in other micro-tidal environments.

## 3. Methods

### 3.1. 3D hydrodynamic model

The prediction of circulation within the Choctawhatchee Bay system must represent the interactions between components driven by tides, winds, and density gradients, as well as their interactions with the complex coastline, bay, and river. The ADvanced CIRCulation (ADCIRC) model is a finite-element, hydrodynamic model that is widely used for tidal and storm surge studies (Luettich et al., 1992; Westerink et al., 2008). It represents the coastal environment via unstructured meshes that can consist of millions of triangular finite elements of varying sizes to describe variations in open water, in the nearshore, and overland. ADCIRC has achieved prominence for predictions of storm surge and coastal flooding (Bunya et al., 2010; Dietrich et al., 2010, 2011; Blanton et al., 2012; Lin et al., 2012; Atkinson et al., 2013;

Bhaskaran et al., 2013; Murty et al., 2014; Passeri et al., 2015; Bilskie et al., 2016), via the use of its depth-averaged, barotropic version. This study will utilize its fully three-dimensional, baroclinic version to predict the plume dynamics near Choctawhatchee Bay.

Previous studies have validated the baroclinic abilities of ADCIRC through idealistic and realistic applications. The former includes the lock exchange or dam break test, in which waters of different densities initially separated by a vertical barrier are allowed to mix, which is representative of the mixing processes that occur frequently in the coastal ocean, such as that of a fresh-water river emptying into a salt water estuary. ADCIRC was able to provide reasonable predictions for the location, thickness, speed and mixing width of the density front for a laboratory lock exchange test (Kolar et al., 2009). Other studies have demonstrated ADCIRC's ability to predict density-driven flows in regions of shallow bathymetry, such as bays, marshes, and channels adjacent to complicated coastlines that may be under-represented in structured global or regional circulation models. One such study involved modeling the two-layer stratified flow conditions in the Turkish Dardanelles Strait that connects the Aegean Sea to the Marmara Sea and the evolution of the Dardanelles Plume (Blain et al., 2009). Open ocean boundary conditions for the ADCIRC model were derived through one-way coupling with a regional HYbrid Coordinate Ocean Model (HYCOM). The coupled ADCIRC-HYCOM model predicted the behavior of the Dardanelles outflow into the Aegean Sea when forced with accurate initial conditions for stratification in the Dardanelles Strait. In another study, a coastal forecast system designed to predict ocean currents near the entrance of Chesapeake Bay was tested with baroclinic ADCIRC as its core circulation model (Blain et al., 2012). Baroclinic ADCIRC was also validated for a larger study area in the NGOM that extended along the Texas, Louisiana, Mississippi, Alabama and Florida coasts (Dresback et al., 2010). The salinity and heat transport predicted by ADCIRC over the model domain, which represented the Mississippi and Louisiana coastal waters in detail, were found to match model results from a structured Gulf of Mexico HYCOM model. In all of these studies, HYCOM represented the coastlines with a typical resolution of 4 km, while ADCIRC's unstructured meshes had maximum resolutions of 50 m, thus allowing a better representation of coastal dynamics.

Recent improvements have advanced ADCIRC's ability to predict basin-wide density-driven flows involving multiple spatial scales and steep bathymetric gradients (Fathi et al., 2019). These algorithmic changes to ADCIRC include: (a) using a higher-order (cubic) interpolation scheme for the accurate computation of the baroclinic pressure gradient term, (b) using a biharmonic operator (Holland, 1978; Zhang and Baptista, 2008) for the viscosity and diffusion coefficients of the momentum and transport equations instead of a Laplacian scheme, which is known to be overly diffusive when multiple spatial scales are involved, (c) adaptive filtering of the velocity at every time step based on a weighted average of the velocity at neighboring nodes to smooth noisy oscillations (Asselin, 1972; Shapiro, 1970), and (d) systematic bathymetry smoothing to prevent numerical instability (Barnier et al., 1998; Sikiric et al., 2009). With these improvements, ADCIRC was successfully applied as a three-dimensional, Gulf-wide baroclinic model to predict conditions in the Gulf for June 2010, during the Deepwater Horizon oil spill event. The model sea surface velocities captured the Loop Current in the Gulf. The sea surface velocities, salinities, and temperatures predicted by ADCIRC were in good agreement with model results from the data-assimilated HYCOM model (Fathi et al., 2019). In the present work, we build on these recent improvements and after minor changes, successfully apply ADCIRC to represent the three dimensional transport and mixing of riverine freshwater in the vicinity of the coastline. A detailed description of the governing equations solved by the ADCIRC 3D code is provided below for completeness.

#### 3.1.1. Three dimensional shallow water equations

ADCIRC solves the three-dimensional, shallow water momentum equations listed below, which are derived from the Navier–Stokes equations after applying the Boussinesq and hydrostatic approximation (Luettich et al., 1992; Luettich and Westerink, 2004; Fathi et al., 2019).

$$\frac{\partial u}{\partial t} + u\frac{\partial u}{\partial x} + v\frac{\partial u}{\partial y} + w\frac{\partial u}{\partial z} - fv = -g\frac{\partial[(\zeta + p_s/g\rho_0 - \alpha\eta)]}{\partial x} + \frac{\partial}{\partial z}\left(\frac{\tau_{zx}}{\rho_0}\right) - b_x + m_x$$

$$\frac{\partial v}{\partial t} + u\frac{\partial v}{\partial x} + v\frac{\partial v}{\partial y} + w\frac{\partial v}{\partial z} + fu = -g\frac{\partial[(\zeta + p_s/g\rho_0 - \alpha\eta)]}{\partial y} + \frac{\partial}{\partial z}\left(\frac{\tau_{zy}}{\rho_0}\right) - b_y + m_y$$

where:

$$\frac{\tau_{zy}}{\rho_0} = E_z\frac{\partial u}{\partial z}; \qquad \frac{\tau_{zy}}{\rho_0} = E_z\frac{\partial u}{\partial z};$$

$$b_x = \frac{g}{\rho_0}\frac{\partial}{\partial x}\int_z^{\zeta}\rho\,dz; \qquad b_y = \frac{g}{\rho_0}\frac{\partial}{\partial y}\int_z^{\zeta}\rho\,dz;$$

$$m_x = -E_h\nabla^2\nabla^2 u; \qquad m_y = -E_h\nabla^2\nabla^2 v;$$

$$E_h = \frac{L^5}{8\pi^3}\sqrt{\Lambda^6|\nabla\omega|^2 + \Lambda_d^6|\nabla\nabla\cdot u_h|^2}$$

$$|\nabla\omega| = \sqrt{\left[\frac{\partial}{\partial x}\left(\frac{\partial v}{\partial x} - \frac{\partial u}{\partial y}\right)\right]^2 + \left[\frac{\partial}{\partial y}\left(\frac{\partial v}{\partial x} - \frac{\partial u}{\partial y}\right)\right]^2},$$

$$|\nabla\nabla\cdot u_h| = \sqrt{\left[\frac{\partial}{\partial x}\left(\frac{\partial u}{\partial x} + \frac{\partial v}{\partial y}\right)\right]^2 + \left[\frac{\partial}{\partial y}\left(\frac{\partial u}{\partial x} + \frac{\partial v}{\partial y}\right)\right]^2}.$$

in which $t$ is time; $\zeta$ is the free surface elevation relative to the geoid; $u$, $v$, $w$ are velocity components in the $x$, $y$, and $z$ coordinate directions, respectively; $g$ is the gravitational acceleration; $f$ is the Coriolis effect; $p_S$ is the atmospheric pressure at the free surface; $\eta$ is the Newtonian equilibrium tide potential; $\alpha$ is the effective Earth elasticity factor; $\rho_0$ is the reference density of water; $E_z$ is the vertical eddy viscosity; $m_x$ and $m_y$ are the horizontal diffusion terms; $b_x$ and $b_y$ terms are the baroclinic pressure gradient terms; $E_h$ is the modified Leith biharmonic horizontal viscosity (Fox-Kemper and Menemenlis, 2013); $L$ denotes local grid spacing; and $\Lambda$ and $\Lambda_d$ are non-dimensional coefficients of $\mathcal{O}(1)$.

ADCIRC uses a terrain-following, generalized $\sigma$-coordinate system to solve the above equations. This involves mapping $(x, y, z, t) \mapsto (x_\sigma, y_\sigma, \sigma, t_\sigma)$ such that:

$$x_\sigma = x,$$
$$y_\sigma = y,$$
$$\sigma = a + \frac{a-b}{H}(z - \zeta)$$
$$t_\sigma = t.$$

where $a = 1$ and $b = -1$ are constants, $H = \zeta + h$ is the total water depth, and $h$ is the bathymetric depth relative to the geoid. To minimize inaccuracies in regions of steep bathymetry, this transformation is not applied for the baroclinic pressure gradient terms $b_x$ and $b_y$, and the horizontal diffusion terms $m_x$ and $m_y$ (Dresback et al., 2002; Fathi et al., 2019), which are computed in a $z$-coordinate system. A Mellor–Yamada level 2.5 turbulence closure model is adopted to compute vertical eddy viscosity and diffusivity. The minimum value for vertical eddy diffusivity is set to be spatially variable.

#### 3.1.2. Transport equation

The time-dependent scalar transport of salinity and temperature is modeled by the following advection–diffusion equation:

$$\frac{\partial c}{\partial t} + u\frac{\partial c}{\partial x} + v\frac{\partial c}{\partial y} + w\frac{\partial c}{\partial z} - \mathcal{D}_h(c, N_h) - \mathcal{D}_v(c, N_v) = 0,$$

where $c$ represents the species that is being transported (i.e. salinity or temperature), $\mathcal{D}_h(c, N_h)$ is the biharmonic horizontal diffusion term, and $\mathcal{D}_v(c, N_v)$ is the vertical diffusion term. Sigma coordinate transformation is applied to all the terms in the transport equation except for the horizontal diffusion term, which is computed in a $z$-coordinate system. The modeled temperature and salinity are then used by ADCIRC to compute the density field according to the polynomial equation of state formulated by McDougall et al. (2003).

### 3.2. Unstructured mesh

The unstructured, finite-element, shelf-scale mesh used in the present study (Fig. 1) is derived from an existing larger Gulf- and Atlantic-wide ADCIRC mesh, which has been validated for tides and storm surge predictions for the coastal regions of Northwest Florida and Alabama (UCF, 2011a,b; Passeri et al., 2015; Bilskie et al., 2016).

#### 3.2.1. Adjustments for Choctawhatchee Bay region

The existing mesh was modified for this study by increasing resolution at the inlet and in the open ocean, adding the Choctawhatchee River, and cutting out a shelf-scale mesh with an offshore boundary located along the 200 m depth contour. Floodplains up to the 3 m contour are maintained around the Choctawhatchee Bay and River. The Choctawhatchee River enters the bay at the east end of the bay. The river's realistic profile is traced from satellite imagery up to the USGS gage at Bruce, Florida. Beyond Bruce, the river is given a simplified 'synthetic' profile, which is devoid of all the irregularities and twists and turns of the real river. The upstream river boundary is located at the USGS gage at Caryville, Florida. River bed elevations were derived from FIS study reports for Walton County (FEMA, 2008, 2010). Mesh resolution varies from approximately 20–30 m at Destin Inlet and Choctawhatchee River, to approximately 100–500 m in the Choctawhatchee Bay, to 1–3 km in the shelf (Fig. 1).

#### 3.2.2. Bathymetry smoothing

Insufficient resolution at regions of steep bathymetric gradients in the ocean can cause inaccuracies and lead to numerical instability (Haney, 1991). To minimize these errors, models can employ bathymetry smoothing (Adcroft et al., 2016; Marshall et al., 1997). In the present study, we use the bathymetry smoothing approach implemented by Fathi et al. (2019). Relevant equations from this work are repeated here for completeness. Smoothing is applied to all regions in the mesh deeper than the 15 m contour. The smoothing utilizes common strategies such as limiting the relative variation of the ocean depth over a grid element (Barnier et al., 1998):

$$\max\ rx_0 = \frac{|h_i - h_j|}{h_i + h_j} \leqslant 0.2,$$

and also limiting the hydrostatic inconsistency (Haney) number (Sikiric et al., 2009):

$$\max\ rx_1 = \frac{|h_i^k - h_j^k + h_i^{k-1} - h_j^{k-1}|}{h_i^k + h_j^k - h_i^{k-1} - h_j^{k-1}} \leqslant 3 \sim 6,$$

where $h_i$ and $h_j$ denote bathymetry at adjacent grid nodes $i$ and $j$, respectively, and $h_i^k$ is the depth of the $k$th $\sigma$-layer from the top surface. To eliminate noisy features that may arise after applying the above criteria, a Gaussian filter is also applied to the mesh bathymetry.

### 3.3. Physical forcings

The ADCIRC model for the Choctawhatchee Bay and River system requires initial and boundary conditions for winds, tides, river discharge, surface heat fluxes, salinities and temperatures.

#### 3.3.1. Winds, tides, and river discharge

Tidal forcing is applied in the model through open ocean boundary conditions and via the tidal potential term and consists of seven harmonic constituents: $K_1$, $O_1$, $Q_1$, $M_2$, $S_2$, $N_2$ and $K_2$. The applied winds and surface pressures are from the North American Mesoscale (NAM) model, which is run by the National Centers for Environmental Prediction (http://www.ncep.noaa.gov/) four times a day at a spatial resolution of about 12 km. NAM winds show good agreement with the measured wind speeds and directions at the NOAA Penscola station (Fig. 3). The upstream river boundary of the synthetic channel is forced with a discharge of 150 $m^3/s$, which was the observed river discharge during SCOPE (Roth et al., 2017).

#### 3.3.2. Salinities, temperatures, and heat fluxes

Open ocean boundaries are forced by vertical salinities and temperatures extracted from HYCOM output (Dresback et al., 2010). HYCOM is a data assimilated, global circulation model that is run operationally by the Naval Research Laboratory for the Gulf of Mexico at a resolution of 1/12 degrees. For the present study, initial conditions for salinities and temperatures are derived from publicly available HYCOM output (http://tds.hycom.org/thredds/dodsC/GOMl0.04/expt_31.0/2013/hrly.html) for most of the model domain. HYCOM utilizes a structured grid that does not extend far into inland regions. Therefore, to initialize estuarine conditions, we relied on vertically-varying salinity and temperature profiles provided by the Choctawhatchee Basin Alliance (CBA) (http://www.basinalliance.org/). HYCOM output and CBA measurements were combined in the following manner. First, HYCOM output is interpolated onto ADCIRC mesh vertices that fall within the HYCOM domain. This initializes all the offshore regions of the ADCIRC mesh. ADCIRC mesh vertices that coincide with CBA measurement locations are then seeded with the measured vertical profiles. This is followed by extrapolation outward from the near-shore and offshore ADCIRC mesh vertices that are already initialized. The "final" near-shore initial conditions reflect a gradual transition from the interpolated offshore HYCOM salinities to measured values inside the bay. Surface heat flux values are derived from HYCOM output, but are disabled in Choctawhatchee River.

### 3.4. Model setup

The simulation period spans the months of November–December 2013 to match the timing of the SCOPE experiment. The model is forced by realistic tides, winds, riverine freshwater discharge, and surface heat flux values for this period. Model runs have a diagnostic phase of 5 days (1–6 November 2013) followed by the prognostic phase through 16 December. In the diagnostic phase, the transport of salinity and temperature is disabled and thus the density field is constant, while tides, winds and river inflow are allowed to spin up (Dresback et al., 2010). Salinities and temperatures are allowed to evolve at the beginning of the prognostic phase, and density gradients begin to drive the flow conditions. The model was run for a 45-day simulation with 21 vertical layers at a time step of 0.5 s.

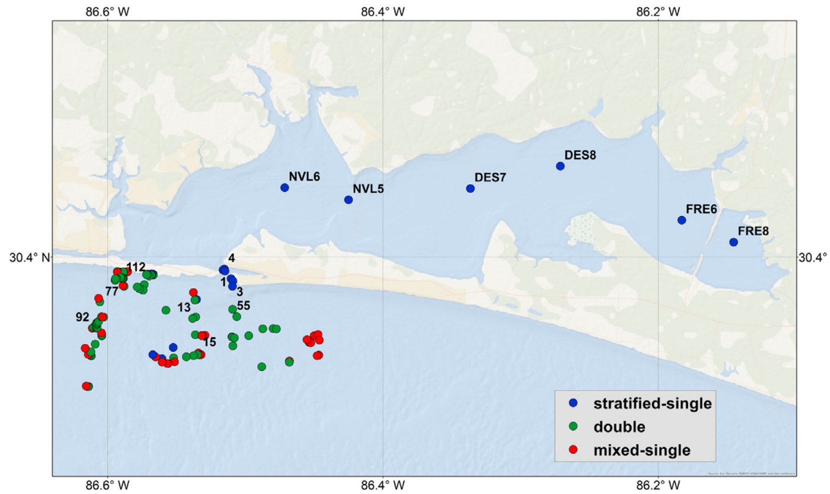


**Fig. 2.** Locations in the bay, inlet, and shelf waters where vertical salinity (circles) and water level observations (asterisks) are available.

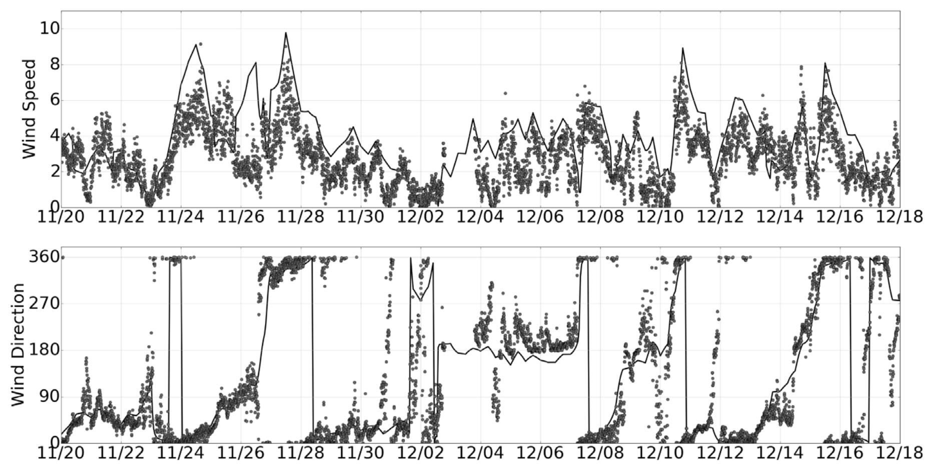


**Fig. 3.** Wind speeds (top panel, in m/s) and directions (bottom panel, in degrees clockwise from north) from 20 November through 17 December 2013 at Pensacola, FL. Gray circles denote observations at NOAA station (ID: 8729840) and black line denotes model forcing.

## 4. Model validation

### 4.1. Water levels

Model water levels are compared against observations (96 h high pass filtered to remove low-frequency oscillations) collected at four locations: Panama City Beach (NOAA station 8729210), Panama City (NOAA station 8729108), SCOPE moored pressure sensor located at 10 m depth off the coast of Beasley Park about 6 to 7 km west of Destin Inlet (MacMahan, 2015a), and SCOPE pressure sensor at the Mid-Bay Bridge in Choctawhatchee Bay (Fig. 4) (MacMahan, 2015b). Overall, observed and modeled water levels are in good agreement, with ADCIRC sometimes underestimating the observed water levels by 0.1 to 0.2 m. There is a slight phase difference between observed and measured water levels at Panama City Beach, likely because the ADCIRC mesh does not extend into the estuary where the NOAA gage is situated. Tidal amplitudes inside Choctawhatchee Bay are attenuated to roughly 30% of the amplitudes at the shelf with a phase delay of 5.5 hours, thus matching the observed behavior (Valle-Levinson et al., 2015).

### 4.2. Vertical salinities

The model's ability to represent the vertical salinity distribution inside the Choctawhatchee Bay and on the shelf were quantified by computing standard error statistics (Wilkin and Hunter, 2013). The error metrics in this study include the Pearson correlation coefficient ($r$):

$$r = \frac{\frac{1}{N}\sum_{i=1}^{N}((o-\langle o\rangle)(m-\langle m\rangle))}{\sigma_m\sigma_o}$$

the centered root mean square error ($E_{CRMS}$):

$$E_{CRMS} = \sqrt{\frac{1}{N}\sum_{i=1}^{N}((m-\langle m\rangle)-(o-\langle o\rangle))^2}$$

and the mean bias ($B_M$):

$$B_M = \langle m\rangle - \langle o\rangle$$

in which $o$ is a set of observed values of size $N$; $m$ is a set of model predictions; $\langle m\rangle$ and $\langle o\rangle$ are the means of $m$ and $o$, respectively; and $\sigma_m$ and $\sigma_o$ are the standard deviations of $m$ and $o$, respectively.

Each metric has its own strengths and limitations in describing model performance. Therefore, it is prudent to use a suite of metrics to avoid an incomplete or limited description of model skill (Koh and Ng, 2012). The correlation coefficient $r$ is a statistical measure of whether the model and observed salinities are related linearly, and it varies from $-1$ (for perfectly negatively correlated), through 0 (for uncorrelated), to $+1$ (for perfectly

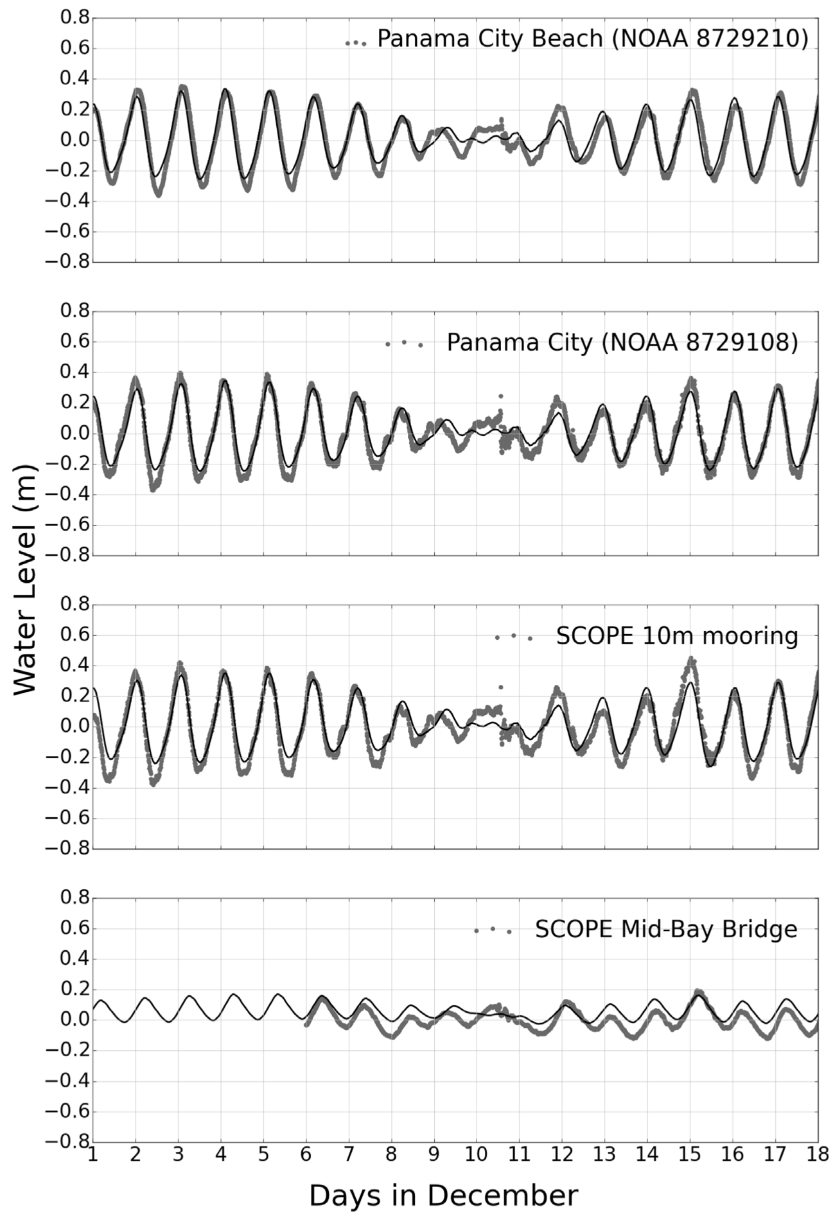


**Fig. 4.** Comparison of observed and modeled water levels. Gray circles denote observations and solid line denotes ADCIRC water levels.

positively correlated). Therefore it quantifies the model's ability to capture the pattern of vertical variability in the measured salinity data. However, it does not provide any information about the amplitude of variability, which is quantified by the standard deviation ($\sigma_m$, $\sigma_o$). The root mean square error is another widely-used estimate of the differences in magnitude between model and observed quantities. It can be resolved into two components, namely differences between the means (mean bias $B_M$) and the differences in their patterns of variation (centered root mean square error $E_{CRMS}$) (Taylor, 2011). The mean bias $B_M$ is a measure of the overall systematic differences between the model and observed salinities and therefore can quantify whether the model is "too high" or "too low". Centered root mean square error compares model and observed quantities after removing any bias associated with their mean values. The $E_{CRMS}$ approaches zero as the modeled and measured profiles become identical. However, a given value of $E_{CRMS}$ can be biased by the amplitude of variations from mean, and thus can be larger when there is a larger variability in the observed profile.

Model salinities are compared against observed vertical salinities at 121 stations, collected between 3–17 December 2013, in the Choctawhatchee Bay and adjacent shelf waters (MacMahan, 2015d) (Fig. 2). These observations show three types of salinity profiles. Observations collected by the Choctawhatchee Basin Alliance inside the bay indicate stratified conditions. In the central and western portions of the bay, observed salinities range from 15 to 20 psu at the surface to about 30 psu at the bottom. Model salinities represent well this large variability in the vertical profile (Fig. 5). At the eastern end, where Choctawhatchee River drains into the bay, the water column is relatively shallow (about 3 m depth) and highly stratified, with a difference of 15 to 20 psu between surface and bottom salinities. Although model salinities also indicate a large difference between surface and bottom salinities (15 psu) they predict well-mixed conditions below the surface layer. Outside the estuary and onto the shelf, the water column is observed to be either well-mixed (see salinity profiles at CTD 15, CTD 92 and CTD 77 in Fig. 6) or has an upper stratified layer and a lower mixed layer (see salinity profiles at CTD 13, CTD 55 and CTD 112 in Fig. 6). Brackish conditions in the surface at the

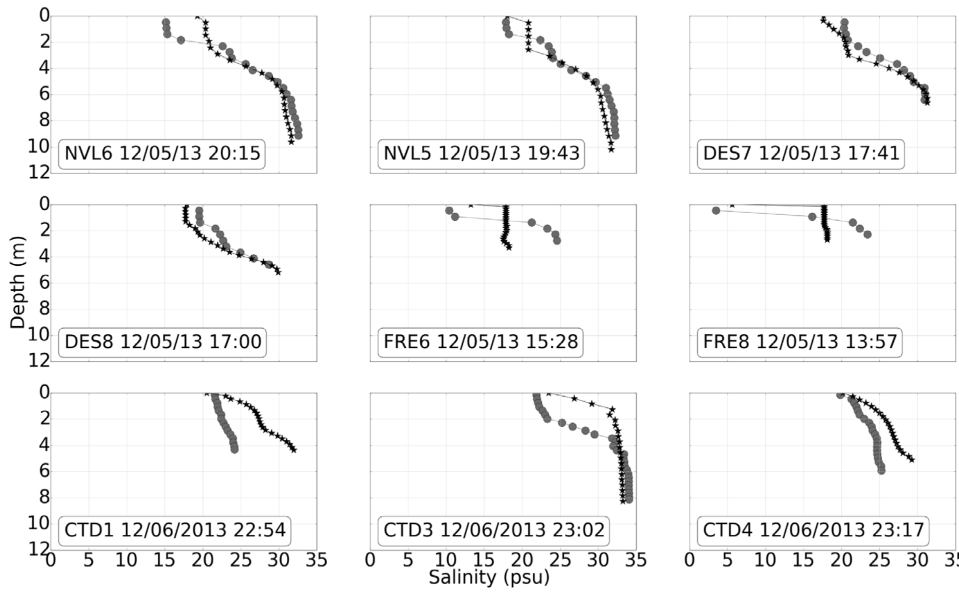


**Fig. 5.** Comparisons of observed (gray circles) and modeled (black asterisks) vertical salinities inside Choctawhatchee Bay (top two panels) and within Destin Inlet (bottom panel), with station locations shown in Fig. 2.

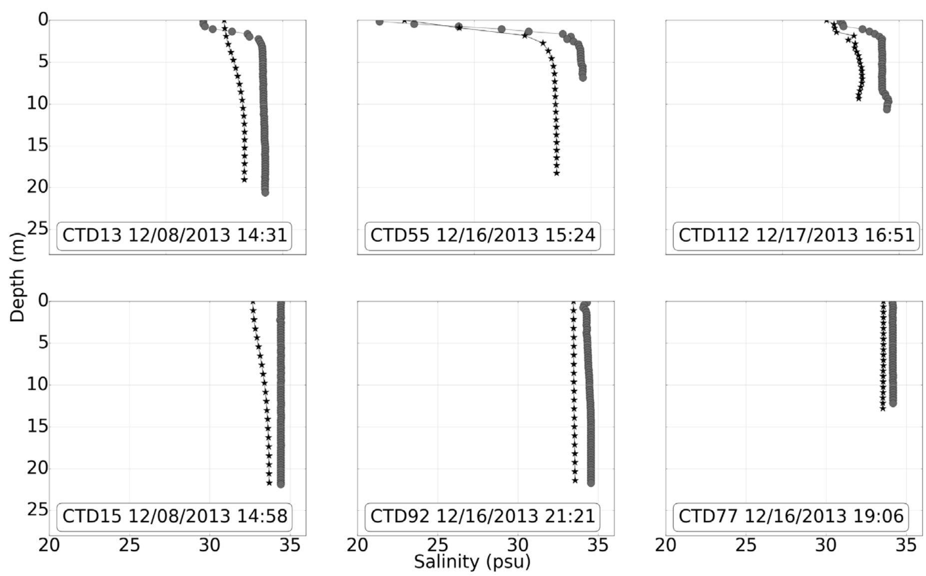


**Fig. 6.** Comparisons of observed (gray circles) and modeled (black asterisks) vertical salinities in the shelf waters adjacent to Choctawhatchee Bay, with station locations shown in Fig. 2.

stations located on the shelf indicate the effects of the surface ebb phase outflow from Destin Inlet.

To characterize their differing geographical location and circulation features, the observed salinity profiles are grouped into three main categories: highly stratified conditions (“single-stratified”), in which the salinities vary through the entire water column; partially stratified conditions (“double”), in which the salinities vary only in an upper layer and are relatively constant in a lower layer; and well-mixed conditions (“single-mixed”), in which the salinities are relatively constant through the entire water column. The “single-stratified” profiles are located typically in shallow waters and in the bay; the “double” profiles are located typically on the shelf near the inlet; and the “single-mixed” profiles are located typically on the shelf far from the inlet. Taken together, these observations provide a comprehensive description of the spatial and temporal variability in the salinity characteristics of the water column in the study area. For “double” profiles, error statistics are computed separately for the upper stratified layer (called “double-stratified”) and the lower mixed layer (called “double-mixed”). For “single-stratified” and “double-stratified” profiles, the model should represent accurately the vertical salinity variability, and thus $r$ is used to quantify this variability.

The error metrics are computed to quantify model performance. We first discuss the error statistics at selected stations (Table 1), which are chosen to be representative of the features of the three categories. At stations DES7, CTD1, and CTD5, (Figs. 5, 6) which are located in the estuary, inlet and inner shelf respectively, the $r$ values are 0.980, 0.960 and 0.802, respectively, signifying a high degree of correspondence between model and observed profiles. Similarly, $r$ can be used to evaluate the model's ability to capture the rapid change in salinities in the “double-stratified” profiles located in the shelf waters. At stations CTD13, CTD 55 and CTD 112, (6) the salinities increase rapidly (2 to 8 psu)

**Table 1**
Error statistics at selected stations.

| Station name | Type | $B_M$ | $E_{CRMS}$ | $r$ | $\sigma_m$ | $\sigma_o$ |
|---|---|---|---|---|---|---|
| DES7 | single-stratified | −1.193 | 1.116 | 0.980 | 4.816 | 4.157 |
| CTD1 | single-stratified | 4.957 | 1.847 | 0.960 | 2.707 | 0.915 |
| CTD5 | single-stratified | 3.686 | 1.078 | 0.802 | 1.765 | 1.190 |
| CTD13 | double-stratified | 0.138 | 0.791 | 0.977 | 0.031 | 0.821 |
| | double-mixed | −1.002 | 0.183 | 0.899 | 0.232 | 0.057 |
| CTD55 | double-stratified | −0.908 | 1.175 | 0.981 | 1.877 | 2.957 |
| | double-mixed | −1.295 | 0.093 | 0.955 | 0.146 | 0.057 |
| CTD112 | double-stratified | −0.851 | 0.440 | 0.811 | 0.214 | 0.595 |
| | double-mixed | −1.015 | 0.146 | 0.237 | 0.149 | 0.049 |
| CTD15 | single-mixed | −1.09 | 0.348 | −0.08 | 0.347 | 0.007 |
| CTD92 | single-mixed | −0.935 | 0.096 | 0.845 | 0.03 | 0.12 |
| CTD77 | single-mixed | −0.597 | 0.015 | −0.803 | 0.008 | 0.008 |

within the top 0 to 2.5 m of the water column . Model and observed salinities in this upper layer are in a good agreement with $r > 0.8$.

The variability in observed salinities can be quantified by the standard deviation, which is very small (less than 0.1 psu) for "double-mixed" and "single-mixed" profiles), signifying a well-mixed water column. Due to this absence of vertical variation, it is meaningful to compare overall differences between modeled and observed salinities, rather than quantifying the degree to which the model can replicate patterns in the observed salinity profile. Therefore, $B_M$ and $E_{CRMS}$ are more appropriate metrics for these profiles. The standard deviation of vertical salinities in the bottom mixed layer at stations CTD 13, CTD 55 and CTD 112 is about 0.05 psu, which indicates almost zero vertical variability. Model salinities are in good agreement with observed mixed-layer salinities at these stations with $E_{CRMS}$ less than $\pm 0.2$ psu and $B_M$ of $\pm 1$ psu. The water column is well-mixed over its entire depth with measured salinities of 34 psu at CTD 15, CTD 92 and CTD 77.

Error metrics are computed at all 121 stations by considering separately the model performance in the stratified and well-mixed portions of the water column (Fig. 7). The water column is observed to be highly-stratified within the estuary, partially stratified in the shelf waters near the inlet and fully mixed with an oceanic salinity of 34 psu several kilometers away from the inlet. When $r$ is high (and approaching $+1.0$), it indicates a high correlation and when $r$ is closer to 0.5, it indicates a moderate correlation (Taylor, 1997, p. 217, Walpole et al., 2012, p. 125). For most of the stratified profiles, the computed $r$ values (see Fig. 7, top left plot) fall within 0.75–1. This indicates a reasonable degree of correlation between modeled and observed vertical salinities. Stratified conditions within the bay and in the upper layers of the shelf waters are therefore well represented by the model. The $B_M$ and $E_{CRMS}$, which are computed for the stratified water column, are largest for stations within the estuary where the water column is highly stratified ($\sigma_o$ between 4 to 6). However, the variability in vertical salinities is captured very well by the model with a high degree of correlation ($r > 0.9$) at these locations. As we move further away from the inlet, the effects of the ebb-phase river plume are minimized and the water column is observed to be well-mixed. The model provides an accurate representation of the well-mixed water column with the $B_M$ being less than 0.5 psu and $E_{CRMS}$ being less than 0.5 psu at these stations. Overall, these statistics indicate that ADCIRC is able to represent well the salinity characteristics in the study area, including the transition from brackish waters in the bay to saline waters on the shelf.

### *4.3. Comparisons to satellite imagery*

In Synthetic Aperture Radar (SAR) images, the convergence zones associated with river plumes are visible as narrow, bright features, and therefore these images are widely used to identify plume footprints (Zheng et al., 2004; Nash and Moum, 2005; Jiayi et al., 2006; Huguenard et al., 2016). SAR images collected during SCOPE, utilizing VV polarization in Stripmap mode with a spatial resolution of 5 m, indicate a distinct ebb-phase river plume at Destin Inlet (Huguenard et al., 2016). It is common in plume modeling to use a single cutoff oceanic salinity to mark the plume boundary. These salinity limits are typically chosen based on local salinity dynamics. For example, Zhao et al. (2018) used 34 psu for Wanquan River, Kourafalou (2001) in the Adriatic sea used 37.8 and 38.4 psu , Choi and Wilkin (2007) chose 32 psu for the Hudson River, Liu et al. (2009) used 29 psu for the Colombia River Plume and Burla et al. (2010) used 28 psu for Colombia River. In the present work, we follow the convention used by Xia et al. (2011) for their analysis of the Perdido Bay Plume located adjacent to Choctawhatchee Bay and use the 33 psu isohaline to define the boundaries of the Choctawhatchee river plume.

It is noted that coastal models are known to underestimate the spreading of a river plume due to limitations in representing the fine-scale turbulent processes that occur at the plume front (Huguenard et al., 2016). Here, we adopt a qualitative approach to investigate model skill in predicting the plume geometry. The boundary of the satellite plume is visually identified and marked by yellow stars in Fig. 8. Overall, the model and observed plume footprints are in good agreement with the cross-shore extent of the plume being underestimated by roughly 1.5 to 2 km in the model (see the red lines vs visible plume extents in Fig. 8).

Model salinities (33-psu salinity contour) during the ebb phase on 3–4 December reveal that, under the influence of weak southerly winds (2 to 4 m/s), the model plume spreads radially onto the shelf and along the coastline. The plume cross-shore extents are roughly 6 km and 4.4 km in the satellite and model plumes, respectively, on 3 December. On 4 December both the model and satellite plume have a similar cross-shore extent of 5 km. The winds continue to be weak and southerly on 5 December. The model and the satellite plume show a preferential expansion toward the west and have a similar cross-shore extent (5 km).

The ebb-phase plume is more restricted to the coastline on 9 December, in the SAR imagery, when the tides are the weakest in the month (neap tides) and the prevailing winds are south-easterly. During this time, the model plume has a slightly larger cross-shore extent (4.2 km) than the satellite plume (3.6 km). On 13 December, winds with moderate wind speeds (6 to 8 m/s) blow predominantly from the north and enhance the offshore spreading of the plume. The 33-psu model salinity contour is located at a distance of 5 km south of the inlet, whereas the maximum cross-shore extent of the plume is roughly 6 km in the satellite image. The model plume, forced by weak northerly winds on 17 December, expands offshore to about 4.37 km south of the inlet, whereas the cross-shore extent of the observed plume is roughly 7 km. The down-shelf spreading in the model plume may be caused by a slight under-estimation of the wind forcing during this period (see the slight mismatch in observed and forced wind speeds on 17 December in Fig. 3). These validation results are an indication that ADCIRC can represent the response of the buoyant plume to wind forcing, and they allow for exploratory studies in a following section. We also acknowledge that although the modeled plume footprint compares favorably with the satellite plume in the near field, the modeled plume boundary is less realistic as we move away from the inlet. As mentioned earlier, modeling satellite plume footprints accurately is a challenging problem (Osadchiev and Zavialov, 2013; Osadchiev, 2015; Huguenard et al., 2016) and we recognize the scope for improvements in the model especially in representing the wind field, background coastal circulation and turbulent mixing properties.

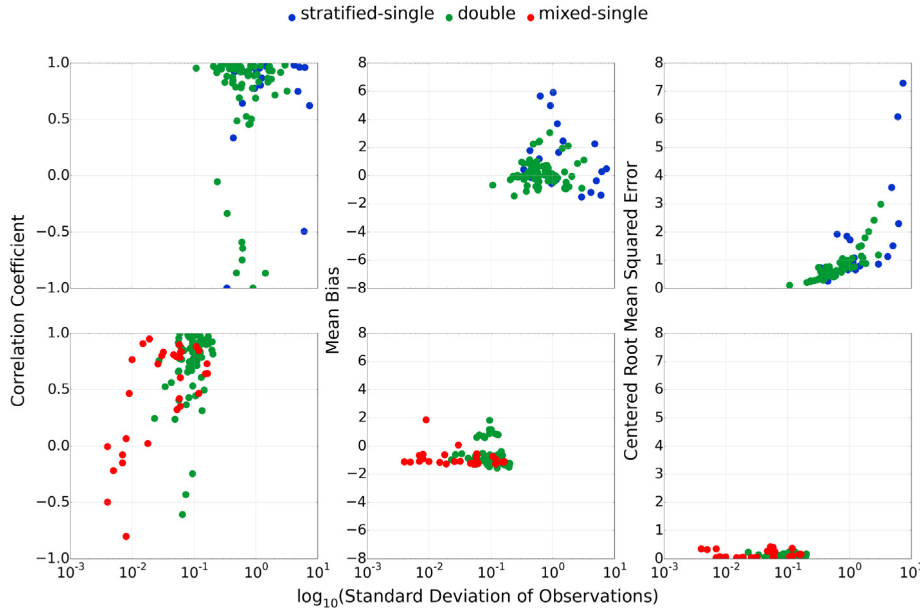


**Fig. 7.** Error statistics (from left to right: correlation coefficient, mean bias and centered root mean squared error) computed for model salinities. Top row corresponds to model skill in stratified conditions. Bottom row corresponds to model skill in well mixed conditions. Blue, green and red circles represent "stratified-single", "double" and "mixed-single" conditions respectively. (For interpretation of the references to color in this figure legend, the reader is referred to the web version of this article.)

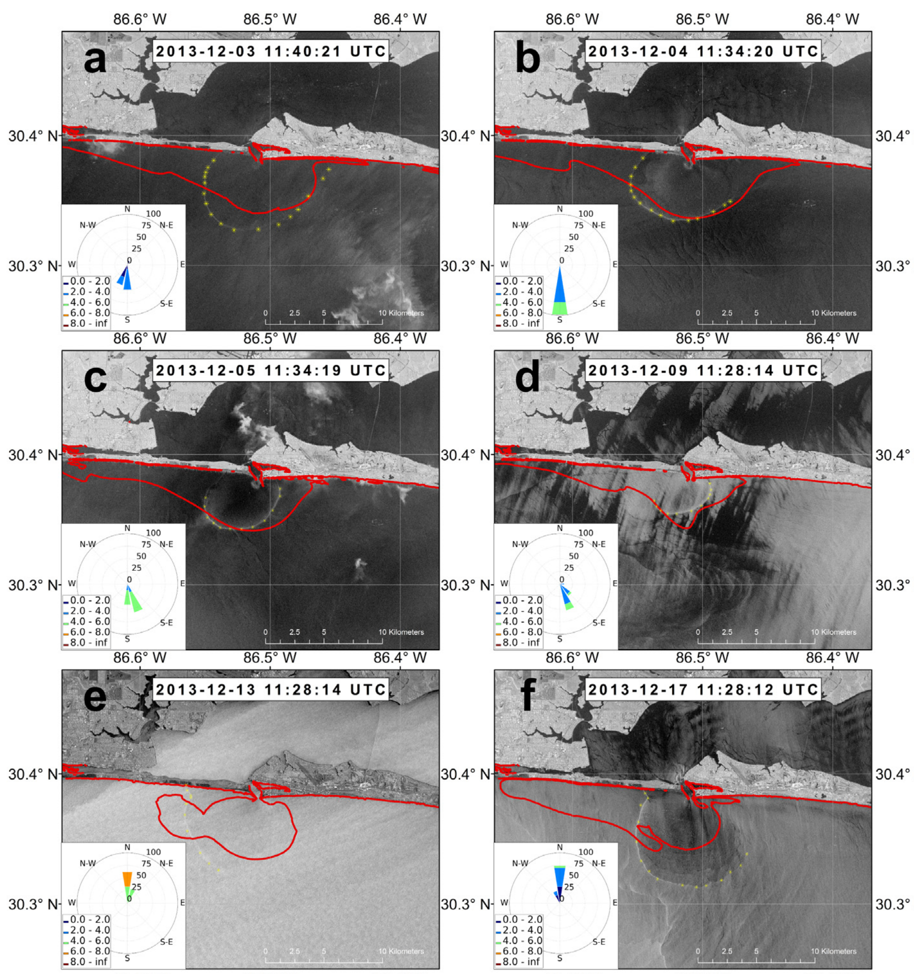


**Fig. 8.** Ebb-phase plume footprint at Destin Inlet observed in SAR satellite imagery (yellow stars) and represented by the 33 psu model salinity contour (red line). Wind roses represent the wind forcing over the past 24 h. (COSMO-SkyMed$^{TM}$ Product ©ASI 2013 processed under license from ASI — Agenzia Spaziale Italiana. All rights reserved. Distributed by e-GEOS. Downlinked and processed by CSTARS.).

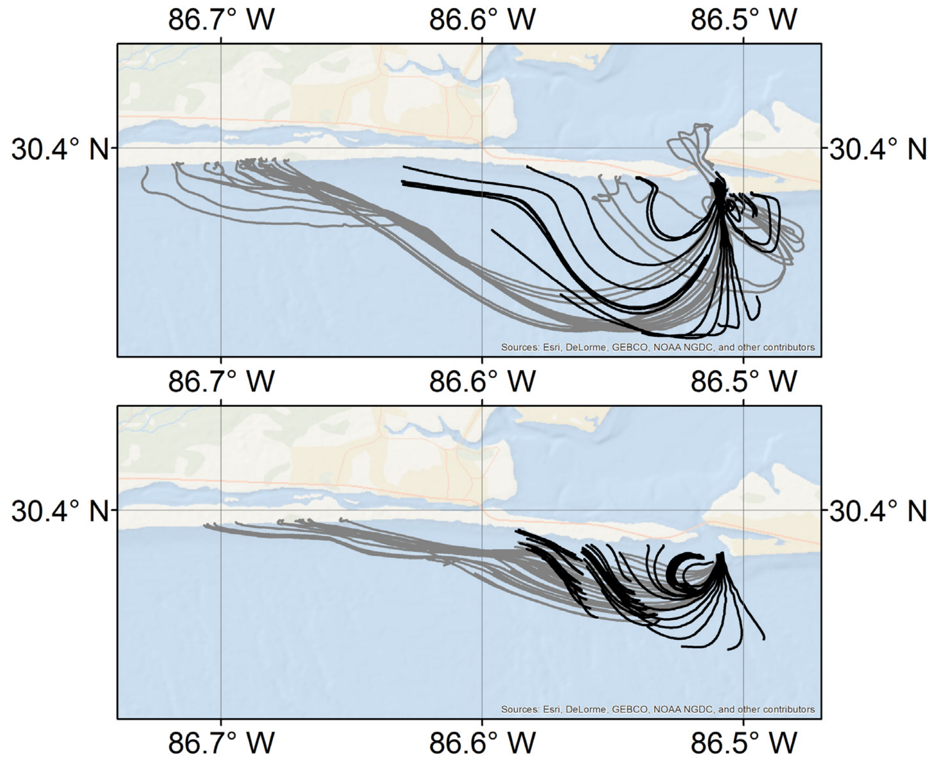


**Fig. 9.** Observed drifter movement (gray lines) and trajectories of Lagrangian particles advected by modeled surface currents (black lines). Drifters are released in the inlet during the ebb-phase on 5 December and 8 December.

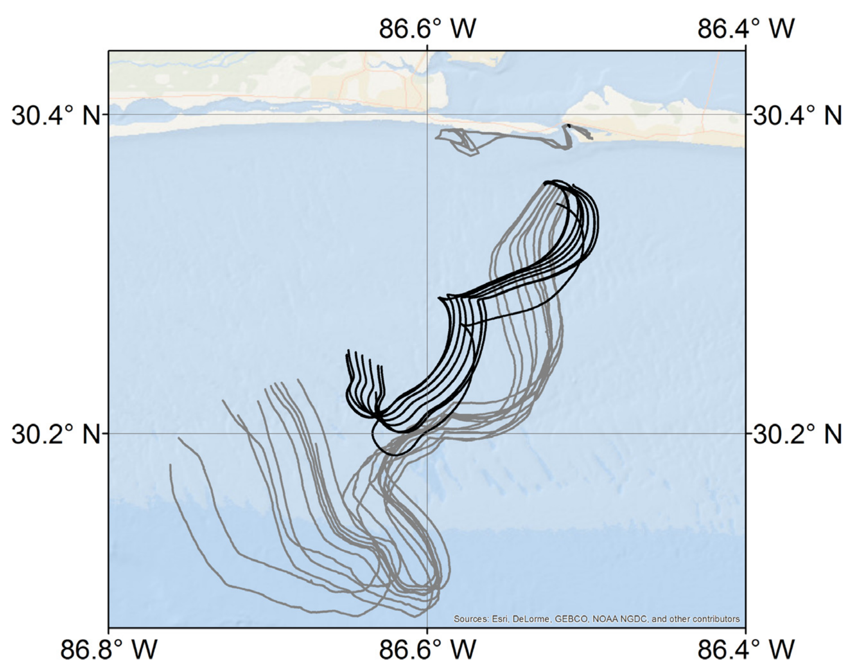


**Fig. 10.** Observed drifter movement (gray lines) and trajectories of Lagrangian particles advected by modeled surface currents (black lines) on 10 December.

### *4.4. Drifter movement*

During SCOPE, drifters were released at the inlet to study surface transport characteristics near the inlet (MacMahan, 2015c). Here, we use Lagrangian particles as a proxy for SCOPE drifters and advect them by modeled surface currents utilizing an existing particle tracking algorithm (Dietrich et al., 2012). Particle trajectories are compared with observed drifter pathways to evaluate model skill in representing nearshore plume- and wind-driven surface currents (Figs. 9 and 10). SCOPE drifters were released at the inlet during the ebb phase of the tidal cycle on 5 December, 8 December and 10 December (Roth et al., 2017). On 5 December, winds are weak and southerly and the drifters first trace an offshore radial bulge as it exits from the inlet before being transported to the west. On 8 December, a moderate easterly component in the prevailing winds force the SCOPE drifters to immediately turn west and proceed along the coast as they exit the inlet. On 10 December, the wind forcing is northerly and moderate and the drifters are advected southward and offshore away from the inlet. As in other studies (Callies et al., 2017; Edwards et al., 2006), it is challenging to represent realistic drifter pathways with model particle trajectories. On 5 December, particles trace a radial bulge and are transported to the west in a manner similar to that observed in the real drifters. However, the modeled currents do not carry the particles as far down the coast as is observed in reality. On 8 December, the particles turn west and proceed along the coastline as soon as they exit the inlet, thus matching the observed drifter behavior. However, these particles beach earlier than the real drifters. On 10 December, the particle movement match the observed drifter movement. Just like the real drifters, the particles do not trace a radial bulge or coastal jet in the vicinity of the inlet and are transported far south by the model currents and winds. Overall, particle trajectories are able to reflect changes in the plume response with changing wind conditions as is being described by the observed drifters. However, the model underestimates the strength of the ambient surface shelf currents during the simulation period, and therefore the model particles do not travel as far as the real drifters. Also, the particle tracking method does not take into account windage effects, which may also be causing inaccuracies in the track predictions.

## 5. Results and discussion

### 5.1. Wind effects on plume geometry

The validated ADCIRC model is now applied to identify the plume response to changing wind conditions (Fig. 11). For this, we identify a period (24–27 November) when the tidal forcing is weak and constant (amplitude of 0.15 m). During this time, passing cold fronts lead to moderately-strong winds (4 to 10 m/s) that undergo a 360° reversal in their directions over a span of 3 to 4 days. The model plume at late-ebb is compared on these days for two scenarios. In the first scenario, the wind forcing is enabled, and therefore model predictions represent the plume response to both tidal and wind forcing mechanisms. In the second scenario, the wind forcing is disabled, and therefore the model predictions indicate how the plume behaves in the absence of wind forcing.

We again consider the 33 psu salinity contour to be representative of the model plume when the winds are enabled. However, when the winds are disabled, the 33 psu salinity contour (dark gray line in Fig. 11a–d) describe a considerably wider plume that stretches for a distance of roughly 20 km along either side of the coastline. This behavior is consistent with a substantially wider model plume reported for the Perdido Bay when wind forcing is disabled (Table 2 in Xia et al., 2011). However, disabling the wind forcing is expected to impact the mixing in the shelf waters. It is not clear whether the 33 psu salinity contour is representative of the current plume or if it describes "plume" remnants from previous tidal cycles that persist due to unrealistic mixing in the model. Due to this uncertainty, when the wind forcing is disabled, we follow a conservative approach and consider the 32 psu (light gray line in Fig. 11a–d) to represent the current plume.

On 24 November (Fig. 11a), prevailing winds that are moderately strong (6 to 8 m/s) and northeasterly force the plume (red line) toward the west of the inlet, with a length of 6.58 km and a width of 9.0 km. In the absence of winds, the plume (light gray line) is nearly symmetrical and expands radially offshore with a slight preference toward the down-shelf direction and has a length of 4.5 km and a width of 6.5 km. On the next day (25 November, Fig. 11b) the winds remain northeasterly but are weaker with a reduced offshore component (2 to 4 m/s). Due to the larger, downwelling-favorable, easterly component in the wind forcing, the down-shelf spreading of the plume (red line) is enhanced, and it stretches along the coastline up to a distance of 7 km from the inlet. The width of the plume signature reduces to 6.5 km on 25 November. The offshore spread of the plume to the south of the inlet is also limited, and the length of the plume (3.6 km) is roughly half of that of the previous day. When the wind forcing is disabled, the plume (light gray line) spreads out in a nearly symmetric manner with a slight preferential motion toward the down-shelf direction and has a cross-shore extent of 4.0 km and an along-shore extent of 5.3 km.

On 26 November (Fig. 11c), the winds have shifted and are blowing from the southeast and becoming southerly with wind speeds between 6 to 8 m/s. These winds prevent the plume (dark red line) from spreading farther offshore and restrict the plume length to be less than 3 km and width to be around 3 km. The plume also exhibits a preferential up-shelf accumulation. In the no-wind scenario, the plume (light gray line) expands radially offshore and spreads along the coastline with a preferential motion toward the west. The plume signature has roughly the same length as the realistic plume forced by both tides and winds.

On 27 November (Fig. 11d), while the wind speeds are similar at 6 to 8 m/s, the winds shift in direction and become northwesterly. The plume signature is significantly different from that of the previous days. The northerly (or offshore) component of the winds enhances the offshore advection and restricts the lateral (east–west) expansion of the plume, causing the length of the plume (8.0 km) to be more than twice its width (3.5 km). The plume signature changes dramatically when the winds are disabled, with the width of the surface plume (light gray line) (4.5 km) being more than twice its length (2.0 km).

Plume geometry at late ebb on consecutive days from 24 November – 17 December was also examined (not shown here). The model plume displayed a radial bulge and down-shelf spreading irrespective of the direction both when the wind forcing was weak (less than 4 m/s) and when the winds were moderate and had a prominent easterly or down-welling component. When the winds were north easterly and the offshore (or northerly) component in the winds was larger, the model plume was detached from the coastline. On the days when the easterly or the downwelling-favorable component was larger, the plume spread along the coastline. When the winds were south-easterly (onshore and downwelling favorable), the plume displayed minor up-shelf accumulation and dominant down-shelf spreading. However, when the wind speeds increased to 6 to 8 m/s, the down-shelf spreading was minimized and the plume remained largely restricted to the coastline with a preferential spreading in the up-shelf direction. Offshore or northerly winds with moderate wind speeds caused the model plume to spread offshore directly southward without any preferential expansion toward either the east or the west.

### 5.2. Tide effects on plume geometry

To analyze tidal effects on the plume geometry, we choose a period when the tides transition from neap to spring and the wind speeds (near-constant between 4 to 6 m/s) and directions (near-constant and northerly) do not show a significant variability. On 28 November, the winds are northerly with wind speeds between 4 to 6 m/s. Tidal forcing is weak and has an amplitude of 0.12 m. The model plume (Fig. 12a) is oriented slightly toward the west and has a length of 4.4 km and width of 3.6 km. On the next day, the winds are weaker (2 to 4 m/s) and northeasterly, and the tidal amplitude increases slightly to 0.13 m. The plume (Fig. 12b) spreads out radially with a length of 4 km and width of 6.0 km. The tides strengthen (to an amplitude of 0.22 m) on 30 November, whereas the wind forcing continue to be weak

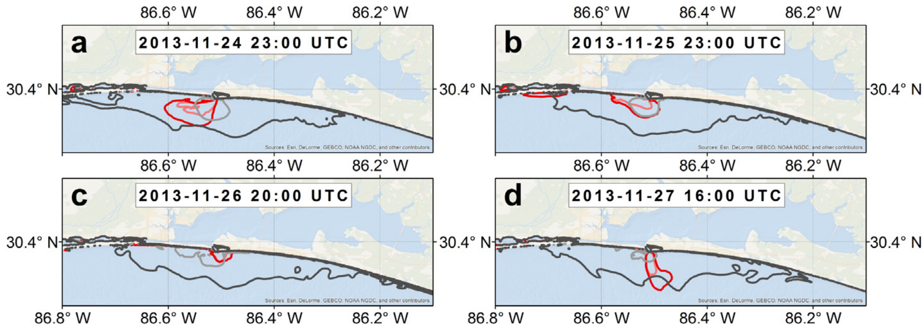


**Fig. 11.** Plume signature described by the 32 (coral and light gray lines) and 33 (red and dark gray lines) psu model salinity contours on 24–27 November overlaid on ArcGIS Map Imagery. Red and coral lines indicate plume response to realistic wind forcing. Gray lines shows model plume behavior when the wind forcing is disabled. (For interpretation of the references to color in this figure legend, the reader is referred to the web version of this article.)

(2 to 4 m/s) and northeasterly. The ebb phase plume (Fig. 12c) is advected farther toward the west along the coastline than in the previous days, and the width of the plume is larger and equal to 7 km. The cross-shore length of the plume is 4.26 km, similar to that of the previous day. The tidal amplitude strengthens further on 1 December to 0.28 m. Wind forcing continues to be weak (2 to 4 m/s) and predominantly northeasterly. The plume (Fig. 12d) spreads along the coastline to the west of Destin as in the previous day. However, the plume signature is larger with a width equal to 10.0 km and a length equal to 6.0 km on 1 December.

Very weak winds (0–2 m/s) blow from the northwest on 2 December. The plume footprint (Fig. 12e) is identical to that of the previous day with an average length of 6.0 km and width of 10.0 km. The tidal amplitude steadily increases to 0.32 m on Dec 3. The plume (Fig. 12f) is forced by weak (2–4 m/s) southerly winds. Although the plume advects to both the east and west of Destin, it remains restricted to the coastline. The plume footprint has a radial bulge south of Destin that has a length of 6.0 km and a width of 8.7 km.

### *5.3. Discussion*

Winter cold fronts bring considerable variability in the wind conditions over the Florida Panhandle and influence the behavior of the ebb phase plume at Destin. Model predictions of salinities show that, during a period of near-constant tidal forcing and moderately strong winds of near-constant magnitude, the plume response can change significantly on consecutive days due to sharp changes in the direction of the prevailing winds. As the easterly or downwelling-favorable component in the wind increases, the plume spreading in the down-shelf direction along the coastline is enhanced. This is in agreement with the behavior of the drifters that was observed by SCOPE researchers in mid- to late-December (Roth et al., 2017). Our findings support their hypothesis that passing cold fronts can create sustained winds with an easterly component multiple times during winter 2013 and cause the ebb-phase plume to form a coastal current west of Destin. Moderate northerly or offshore winds enhance the cross-shore expansion of the plume, whereas southerly or onshore winds restrict the plume to the coastline. These results in a realistic model are also similar to the response of the adjacent Perdido Bay plume to idealized on-shore and off-shore wind conditions (Xia et al., 2011) and match expected plume response to wind forcing. The separation between the 32 and 33 psu salinity contours (coral and red lines in Fig. 11) indicate that whenever there is an offshore component in the winds (panels a, b and (d), there is a gradual transition in model salinities across the plume front, whereas when the winds are onshore (panel (c), there is a sharp salinity gradient across the plume front.

Wind speeds during 24–27 November are larger than 4 m/s and are therefore expected to influence plume dynamics in the near-field according to the criteria to delineate non-wind- and wind-forced conditions (Kakoulaki et al., 2014). Therefore, we expect a considerable difference in the model plume footprint when the winds are disabled and all other conditions remain the same. Model salinities reveal that the plume expands radially out of the inlet with a preferential down-shelf spreading in the absence of wind forcing. The size of the model plume is insensitive to the presence and absence of winds (except in the case of prevailing northerly winds) and is in contrast to the behavior of the Perdido Bay plume, whose surface plume area, length, and width are smaller when forced by idealized wind conditions than without wind forcing (Xia et al., 2011). This behavior is attributed to the application of the 32 psu salinity contour to describe the model plume when the wind forcing is disabled, which might be causing an underestimation of the plume extent.

Ebb phase brackish outflows that enter the continental shelf are expected to turn right in the northern hemisphere and form a coastal current that extends down coast due to the influence of Earth's rotation (Shi et al., 2010; Xia et al., 2007). The Kelvin number is used to quantify the relative importance of rotation effects on a river plume (Dzwonkowski and Yan, 2005). When the Kelvin number is $\ll 1$ the impact of Coriolis force on plume dynamics is considered to be small. Due to the narrow geometry of Destin Inlet, the Choctawhatchee Bay plume is a small-scale river plume, with Kelvin number equal to 0.1 (Roth et al., 2017). Therefore, the effect of the Earth's rotation is less pronounced for the Choctawhatchee Bay plume. In the absence of wind forcing, river plumes in the northern hemisphere are expected to form a recirculating bulge at the inlet and propagate down-shelf in a coastal current. However, for smaller plumes exiting narrow river mouths, the down-shelf spreading is expected to be less prominent (Fong and Geyer, 2002). The model plume (described by the 32 psu salinity contour) at Destin when the wind forcing is disabled forms a distinct bulge at Destin inlet with a slight preferential spreading toward the west and matches these expectations. Model tidal amplitudes decrease to less than 0.10 m between 26 and 27 November. The plume width is thus slightly smaller on these days, when wind forcing is disabled, than in the previous days.

As the tides transition from neap to spring tides from 28 November to 3 December, the model plume grows in size. Under near-constant wind forcing, the length of the plume steadily increases from 4 to 6.0 km as the tidal amplitude increases from 0.12 to 0.31 m. There is an initial increase in the plume width as the tidal amplitudes change. However, the width of the plume remains constant (9 to 10.0 km) when the tidal amplitude is larger than 0.28 m.

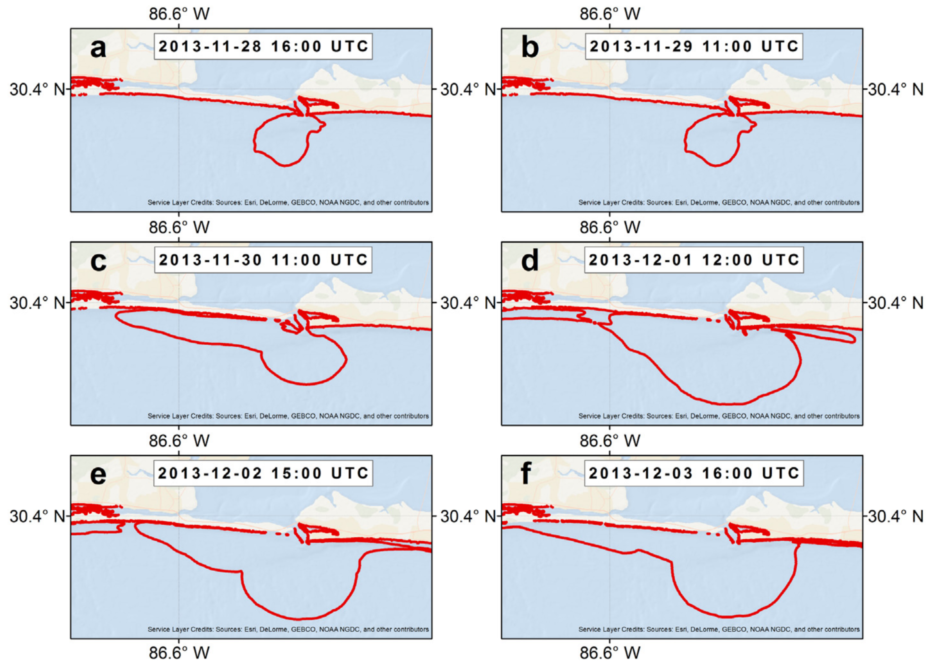


**Fig. 12.** Model plume signature described by the 33 psu salinity contour (red line) during a period of neap-to-spring variability in the tides (28 November to 3 December) overlaid on ArcGIS Map Imagery.

## 6. Conclusions

A recently-enhanced, three-dimensional, baroclinic version of ADCIRC was applied after improvements for high-resolution simulations of the mixing and transport of fresh water at the river-estuarine-shelf scale. The model was used to represent the wind- and density-driven circulation inside Choctawhatchee Bay and adjacent shelf waters, which is representative of several micro-tidal estuaries along the northern Gulf of Mexico coastline. Model performance was evaluated by comparisons with observed tides, vertical salinity profiles and satellite imagery.

The validated model was then applied to study the response of ebb phase brackish plume at Destin to variability in the applied tidal and wind forcing. As noted in Section 1, there are remaining questions about how the Choctawhatchee Bay plume geometry will react to passing cold fronts and spring–neap transitions. Our findings can be summarized as follows:

1. *ADCIRC represents well the surface transport of the plume in realistic geometry and with varying tides and winds.* The water levels were shown to be within 0.1 to 0.2 m of observations at the tide stations, and the vertical salinities were shown to be predicted well at both the stratified (with correlation $r > 0.75$) and well-mixed (with $E_{CRMS} < 0.5$ and $B_M < 2$ psu) observed profiles. The model predictions were also a good match to the qualitative behavior of the plume as observed in satellite imagery, and of surface drifters released during SCOPE. Overall, our validation efforts indicate that the model shows comparable skill to other models in capturing the key features of a small scale plume, especially in the near field. Future studies will explore improving model performance by using more accurate initial conditions, wind fields and more realistic parameters to represent turbulent mixing.
2. *In the absence of winds, the Choctawhatchee Bay plume has a size proportional to the tidal amplitude and expands radially out of Destin Inlet with a preferential down-shelf spreading.* The cross-shore extent (length) of the plume is typically smaller than the alongshore extent (width), with lengths of 2 to 4.5 km and widths of 4.5 to 6.5 km. The plume length increases with a larger tidal amplitude, but its width remains constant for tidal amplitudes larger than 0.28 m. In most cases, when the wind forcing is weak, the plume turns to the right and spreads down-shelf. This behavior is expected, as the plume can be classified as a small-scale river plume with Kelvin number equal to 0.1.
3. *The cross-shore extent (length) of the plume can vary with tidal amplitudes and sustained northerly or southerly winds.* Local wind data collected during SCOPE indicate that cross-shore winds (northerly or southerly) are most frequent with the strongest winds being northerly. The length of the plume is maximized (8.0 km) when spring tides combine with moderate northerly winds. The plume length is minimized (2.0 km) when neap tides combine with southerly winds.
4. *The alongshore extent (width) of the plume can be increased significantly for winds with an easterly component.* Relatively infrequently, the area is also subject to alongshore winds, which are typically from the east and northeast with magnitudes of about 5 m/s. The width of the plume is largest (9.0–10 km) when spring tides combine with weak winds or when moderate winds with an easterly component cause a westward expansion of the plume.

This analysis provides new insights into the spatial and temporal scales of variability in the Choctawhatchee Bay plume signature as it responds to changing tidal and wind forcing. Based on our findings, we expect the plume to be narrow and spread directly offshore on most days and propagate down-shelf as a coastal current relatively less frequently.

Like in other river-dominated estuaries, the Choctawhatchee Bay plume plays a vital role in the sustenance of the bay ecosystem. It facilitates the offshore transport of surface material such as fish larvae, phytoplankton and pollutants out of the bay and the inlet into the continental shelf and can prevent offshore chemical and oil pollutants from beaching. Therefore, understanding the variability in the east–west and north–south extents of the plume under different environmental forcing scenarios can provide useful guidance for local fisheries management and pollution control activities. The trends identified in this work have broader applicability and can be applied to estimate surface plume response to weather phenomenon in other micro-tidal estuaries, especially those that have a limited connectivity to the open ocean.

## Declaration of competing interest

The authors declare that they have no known competing financial interests or personal relationships that could have appeared to influence the work reported in this paper.

## CRediT authorship contribution statement

**R. Cyriac:** Methodology, Formal analysis, Writing - original draft. **J.C. Dietrich:** Conceptualization, Writing - review & editing, Funding acquisition. **C.A. Blain:** Methodology, Supervision. **C.N. Dawson:** Resources, Project administration, Funding acquisition. **K.M. Dresback:** Methodology, Software, Supervision. **A. Fathi:** Software, Resources, Supervision. **M.V. Bilskie:** Resources. **H.C. Graber:** Resources. **S.C. Hagen:** Resources. **R.L. Kolar:** Methodology, Supervision.

## Acknowledgments

This work was made possible by grants from the Gulf of Mexico Research Initiative through the Consortium for Advanced Research on Transport of Hydrocarbon in the Environment. Data are publicly available through the Gulf of Mexico Research Initiative Information & Data Cooperative (GRIIDC) at https://data.gulfresearchinitiative.org/data/R6.x806.000:0024 (Cyriac and Dietrich, 2020). We thank the Choctawhatchee Basin Alliance for providing us with observed monthly salinity data in Choctawhatchee Bay. This work used the Extreme Science and Engineering Discovery Environment (Towns et al., 2014), which is supported by National Science Foundation grant number ACI-1548562, specifically the Stampede2 supercomputer at the Texas Advanced Computing Center via the allocation TG-DMS080016N. Co-author Dawson acknowledges the support of the King Abdullah University of Science and Technology, Saudi Arabia Office of Sponsored Research under award number OSR-CRG2018-3711.

## References

Adcroft, A., Campin, J.M., Dutkiewicz, S., Evangelinos, C., Ferreira, D., Forget, G., Fox-Kemper, B., Heimbach, P., Hill, C., Hill, E., Hill, H., Jahn, O., Losch, M., Marshall, J., Maze, G., Menemenlis, D., Molod, A., 2016. MITgcm User Manual. Tech. rep.. MIT Department of EPAS, Cambridge, MA.

Androulidakis, Y.S., Kourafalou, V.H., 2011. Evolution of a buoyant outflow in the presence of complex topography: The dardanelles plume (North Aegean Sea). J. Geophys. Res. Ocean. 116 (C4).

Asselin, R., 1972. Frequency filter for time integrations. Mon. Weather Rev. 100, 487–490.

Atkinson, J.H., Smith, J.M., Bender, C., 2013. Sea-level rise effects on storm surge and nearshore waves on the Texas coast: Influence of landscape and storm characteristics. J. Waterw. Port Coast. Ocean Eng. 139, 98–117.

Barnier, B., Marchesiello, P., De Miranda, A.P., Molines, J.M., Coulibaly, M., 1998. A sigma–coordinate primitive equation model for studying the circulation in the South Atlantic. Part I: Model configuration with error estimates. Deep-Sea Res. I 45 (4–5), 543–572.

Bhaskaran, P.K., Nayak, S., Bonthu, S.R., Murthy, P.L.N., Sen, D., 2013. Performance and validation of a coupled parallel ADCIRC-SWAN model for THANE cyclone in the Bay of Bengal. Environ. Fluid Mech. 13, 601–623.

Bilskie, M.V., Hagen, S.C., Medeiros, S.C., Cox, A.T., Salisbury, M., Coggin, D., 2016. Data and numerical analysis of astronomic tides, wind–waves, and hurricane storm surge along the Northern Gulf of Mexico. J. Geophys. Res. Ocean. 121 (5), 3625–3658.

Blain, C.A., Cambazoglu, M.K., Kourafalou, V.H., 2009. Modeling the Dardanelles strait outflow plume using a coupled model system. In: OCEANS 2009. pp. 1–8.

Blain, C.A., Cambazoglu, M.K., Linzell, R.S., Dresback, K.M., Kolar, R.L., 2012. The predictability of near-coastal currents using a baroclinic unstructured grid model. Ocean Dyn. 62 (3), 411–437.

Blanton, B.O., McGee, J., Fleming, J.G., Kaiser, C., Kaiser, H., Lander, H., Luettich, R.A., Dresback, K.M., Kolar, R.L., 2012. Urgent computing of storm surge for North Carolina's Coast. In: Proceedings of the International Conference on Computational Science, vol. 9, pp. 1677–1686.

Bunya, S., Dietrich, J.C., Westerink, J.J., Ebersole, B.A., Smith, J.M., Atkinson, J.H., Jensen, R.E., Resio, D.T., Luettich, R.A., Dawson, C.N., Cardone, V.J., Cox, A.T., Powell, M.D., Westerink, H.J., Roberts, H.J., 2010. A high-resolution coupled riverine flow, tide, wind, wind wave and storm surge model for southern louisiana and mississippi: Part I – model development and validation. Mon. Weather Rev. 138, 345–377.

Burla, M., Baptista, A.M., Zhang, Y., Frolov, S., 2010. Seasonal and interannual variability of the Columbia River plume: A perspective enabled by multiyear simulation databases. J. Geophys. Res. Ocean. 115 (C2).

Callies, U., Groll, N., Horstmann, J., Kapitza, H., Klein, H., Maßmann, S., Schwichtenberg, F., 2017. Surface drifters in the German Bight: model validation considering windage and Stokes drift. Ocean Sci. 13 (5), 799–827.

Chant, R.J., Wilkin, J., Zhang, W., Choi, B., Hunter, E., Castelao, R., Glenn, S., Jurisa, J., Schofield, O., Houghton, R., Kohut, J., Frazer, T.K., Moline, M.A., 2008. Dispersal of the hudson river plume in the new york bight: Synthesis of observational and numerical studies during latte. Oceanography 21.

Choi, B., Wilkin, J.L., 2007. The effect of wind on the dispersal of the hudson river plume. J. Phys. Oceanogr. 37, 1878–1897.

Cyriac, R., Dietrich, J.C., 2020. CARTHE-III: 3D ADCIRC simulations of salinity transport near Choctawhatchee Bay and Destin Inlet. Distributed by: Gulf of Mexico Research Initiative Information and Data Cooperative (GRIIDC), Harte Research Institute, Texas A&M University – Corpus Christi. Available from: https://data.gulfresearchinitiative.org/data/R6.x806.000:0024.

Cyriac, R., Dietrich, J.C., Fleming, J.G., Blanton, B.O., Kaiser, C., Dawson, C.N., Luettich, R.A., 2018. Variability in coastal flooding predictions due to forecast errors during hurricane arthur (2014). Coast. Eng. 137, 59–78.

Dietrich, J.C., Bunya, S., Westerink, J.J., Ebersole, B.A., Smith, J.M., Atkinson, J.H., Jensen, R.E., Resio, D.T., Luettich, R.A., Dawson, C.N., Cardone, V.J., Cox, A.T., Powell, M.D., Westerink, H.J., Roberts, H.J., 2010. A high-resolution coupled riverine flow, tide, wind, wind wave and storm surge model for southern Louisiana and Mississippi: part II – Synoptic description and analysis of Hurricanes Katrina and Rita. Mon. Weather Rev. 138, 378–404.

Dietrich, J.C., Trahan, C.J., Howard, M.T., Fleming, J.G., Weaver, R.J., Tanaka, S., Yu, L., Luettich, R.A., Dawson, C.N., Westerink, J.J., Wells, G., Lu, A., Vega, K., Kubach, A., Dresback, K.M., Kolar, R.L., Kaiser, C., Twilley, R.R., 2012. Surface Trajectories of Oil Transport along the Northern Coastline of the Gulf of Mexico. Cont. Shelf Res. 41, 17–47.

Dietrich, J.C., Westerink, J.J., Kennedy, A.B., Smith, J.M., Jensen, R.E., Zijlema, M., Holthuijsen, L.H., Dawson, C.N., Luettich, R.A., Powell, M.D., Cardone, V.J., Cox, A.T., Stone, G.W., Pourtaheri, H., Hope, M.E., Tanaka, S., Westerink, L.G., Westerink, H.J., Cobell, Z., 2011. Hurricane Gustav (2008) waves and storm surge: Hindcast, validation and synoptic analysis in southern Louisiana. Mon. Weather Rev. 139, 2488–2522.

Dresback, K.M., Blain, C.A., Kolar, R.L., 2002. Methods to compute baroclinic pressure gradients in FE models, In: Spaulding, M.L., Bedford, K. (Eds.), Proceedings of the 7th International Conference, Estuarine and Coastal Modeling, pp. 103–119.

Dresback, K.M., Kolar, R.L., Blain, C.A., Szpilka, C.M., Szpilka, A.M., Luettich, R.A., Shay, T., 2010. Development and application of the coupled HYCOM and ADCIRC system. In: Estuarine and Coastal Modeling. In: Proceedings of the 11th International Conference, vol. 388, pp. 259–277.

Dzwonkowski, B., Park, K., Collini, R., 2015. The coupled estuarine-shelf response of a river-dominated system during the transition from low to high discharge. J. Geophys. Res. Ocean. 120 (9), 6145–6163.

Dzwonkowski, B., Yan, X., 2005. Tracking of a chesapeake Bay estuarine outflow plume with satellite-based ocean color data. Cont. Shelf Res. 25 (16), 1942–1958.

Edwards, K.P., Werner, F.E., Blanton, B.O., 2006. Comparison of observed and modeled drifter trajectories in coastal regions: An Improvement through adjustments for observed drifter slip and errors in wind fields. J. Atmos. Ocean. Technol. 23 (11), 1614–1620.

Falcieri, F.M., Benetazzo, A., Sclavo, M., Russo, A., Carniel, S., 2013. Po river plume pattern variability investigated from model data. Cont. Shelf Res. 87, 84–95.

Fathi, A., Dietrich, J.C., Dawson, C.N., Dresback, K.M., Samii, A., Cyriac, R., Blain, C.A., Kolar, R.L., 2019. Prediction of surface oil transport in the northern gulf of mexico by using a three-dimensional high-resolution unstructured-grid baroclinic circulation model. Comput. Methods Appl. Mech. Engrg. (in preparation).

FEMA, 2008. Flood Insurance Study, Walton County, Florida. Tech. rep.. Federal Emergency Management Agency.

FEMA, 2010. Flood Insurance Study, Walton County, Florida. Tech. rep.. Federal Emergency Management Agency.

Feng, Z., Li, C., 2010. Cold–front–induced flushing of the Louisiana Bays. J. Mar. Syst. 82 (4), 252–264.

Fong, D.A., Geyer, W.R., 2001. Response of a river plume during an upwelling favorable wind event. J. Geophys. Res. 106, 1067–1084.

Fong, D.A., Geyer, W.R., 2002. The alongshore transport of freshwater in a surface-trapped river plume. J. Phys. Oceanogr. 32, 957–972.

Fox-Kemper, B., Menemenlis, D., 2013. Can large eddy simulation techniques Improve mesoscale rich ocean models ? In: Ocean Modeling in an Eddying Regime. American Geophysical Union, pp. 319–337.

Garvine, R.W., 1995. A dynamical system for classifying buoyant coastal discharges. Cont. Shelf Res. 15, 1585–1596.

Greer, A.T., Shiller, A.M., Hofmann, E.E., Wiggert, J.D., Warner, S.J., Parra, S.M., Pan, C., Book, J.W., Joung, D., Dykstra, S., Krause, J.W., Dzwonkowski, B., Soto, I.M., Cambazoglu, M.K., Deary, A.L., Briseno-Avena, C., Boyette, A.D., Kastler, J.A., Sanial, V., Hode, L., Nwankwo, U., Chiaverano, L.M., Brien, S.J.O., Fitzpatrick, P.J., Lau, Y.H., Dinniman, M.S., Martin, K.M., Ho, P., Mojzis, A.K., Howden, S.D., Hernandez, F.J., Church, I., Miles, T.N., Sponaugle, S., Moum, J.N., Arnone, R.A., Cowen, R.K., Jacobs, G.A., Schofield, O., Graham, W.M., 2018. Functioning of coastal river–dominated ecosystems and implications for oil spill response: From observations to mechanisms and models. Oceanography.

Guo, X., Valle-Levinson, A., 2007. Tidal effects on estuarine circulation and outflow plume in the Chesapeake Bay. Cont. Shelf Res. 27 (1), 20–42.

Handley, L., Altsman, D., DeMay, R. (Eds.), 2007. Seagrass Status and Trends in the Northern Gulf of Mexico: 1940–2002. U. S. Geological Society, pp. 143–153, Scientific Investigations Report 2006–5287.

Haney, R.L., 1991. On the pressure gradient force over steep topography in sigma coordinate ocean models. J. Phys. Oceanogr. 21 (4), 610–619.

Holland, W.R., 1978. The role of mesoscale eddies in the general circulation of the ocean–numerical experiments using a wind-driven quasi–geostrophic model. J. Phys. Oceanogr. 8 (3), 363–392.

Huguenard, K.D., Bogucki, D.J., Ortiz-Suslow, D.G., Laxague, N.J.M., MacMahan, J., Ozgokmen, T.M., Haus, B.K., Reniers, A.J.H.M., Hargrove, J., Soloviev, A.V., Graber, H., 2016. On the nature of the frontal zone of the Choctawhatchee Bay plume in the Gulf of Mexico. J. Geophys. Res. Ocean. 121 (2), 1322–1345.

Janzen, C.D., Wong, K.C., 2002. Wind-forced dynamics at the estuary-shelf interface of a large coastal plain estuary. J. Geophys. Res. Ocean. 107 (C10), 2–1–2–12.

Jiayi, P., David, J.A., Orton, P.M., 2006. Analyses of internal solitary waves generated at the Columbia River plume front using SAR imagery. J. Geophys. Res. Ocean. 112.

Johnson, D.R., Weidemann, A., Arnone, R., Davis, C.O., 2001. Chesapeake Bay outflow plume and coastal upwelling events: Physical and optical properties. J. Geophys. Res. Ocean. 106 (C6), 11613–11622.

Jurisa, J.T., Chant, R., 2012. The coupled hudson river estuarine-plume response to variable wind and river forcings. Ocean Dyn. 62 (5), 771–784.

Kakoulaki, G., MacDonald, D., Horner-Devine, A.R., 2014. The role of wind in the near field and midfield of a river plume. Geophys. Res. Lett. 41 (14), 5132–5138.

Koh, T., Ng, J.S., 2012. Improved diagnostics for NWP verification in the tropics. J. Geophys. Res.: Atmos. 114 (D12).

Kolar, R.L., Kibbey, T.C.G., Szpilka, C.M., Dresback, K.M., Tromble, E.M., Toohey, I.P., Hoggan, J.L., Atkinson, J.H., 2009. Process–oriented tests for validation of baroclinic shallow water models: the lock–exchange problem. Ocean Model. 28, 137–152.

Kourafalou, V.H., 2001. River plume development in semi-enclosed Mediterranean regions: North adriatic sea and northwestern Aegean Sea. J. Mar. Syst. 30 (3), 181–205.

Kuitenbrouwer, D., Reniers, A., MacMahan, J., Roth, M.K., 2018. Coastal protection by a small scale river plume against oil spills in the Northern Gulf of Mexico. Cont. Shelf Res. 163, 1–11.

Lin, N., Emmanuel, K., Oppenheimer, M., Vanmarcke, E., 2012. Physically based assessment of hurricane surge threat under climate change. Nature Clim. Change 2, 462–467.

Liu, Y., MacCready, P., Hickey, B.M., 2009. Columbia river plume patterns in summer 2004 as revealed by a hindcast coastal ocean circulation model. Geophys. Res. Lett. 36 (2).

Luettich, R.A., Westerink, J.J., 2004. Formulation and Numerical Implementation of the 2D/3D ADCIRC Finite Element Model Version 44.XX. University of North Carolina at Chapel Hill, http://adcirc.org/adcirc_theory_2004_12_08.pdf.

Luettich, R.A., Westerink, J.J., Scheffner, N.W., 1992. ADCIRC: An Advanced Three-Dimensional Circulation Model for Shelves Coasts and Estuaries, Report 1: Theory and Methodology of ADCIRC-2DDI and ADCIRC- 3DL. Tech. rep.. United States Army Corps of Engineers.

MacMahan, J., 2015a. SCOPE experiment cross-shore array measurements, Santa Rosa Island, Florida, December 2013. Distributed by: Gulf of Mexico Research Initiative Information and Data Cooperative (GRIIDC), Harte Research Institute, Texas A&M University – Corpus Christi, https://data.gulfresearchinitiative.org/data/R1.x134.073:0008.

MacMahan, J., 2015b. SCOPE Experiment pressure, Choctawhatchee Bay, Florida, December 2013. Distributed by: Gulf of Mexico Research Initiative Information and Data Cooperative (GRIIDC), Harte Research Institute, Texas A&M University – Corpus Christi, https://data.gulfresearchinitiative.org/data/R1.x134.073:0026.

MacMahan, J., 2015c. SCOPE experiment surface drifters, Santa Rosa Island, Florida, December 2013. Distributed by: Gulf of Mexico Research Initiative Information and Data Cooperative (GRIIDC), Harte Research Institute, Texas A&M University – Corpus Christi, https://data.gulfresearchinitiative.org/data/R1.x134.073:0023.

MacMahan, J., 2015d. Surfzone coastal oil pathways experiment (SCOPE) CTD casts near Santa Rosa Island, Florida, December 2013. Distributed by: Gulf of Mexico Research Initiative Information and Data Cooperative (GRIIDC), Harte Research Institute, Texas A&M University – Corpus Christi, https://data.gulfresearchinitiative.org/data/R1.x134.073:0031.

Marshall, J., Adcroft, A., Hill, C., Perelman, L., Heisey, C., 1997. A finite-volume, incompressible Navier Stokes model for studies of the ocean on parallel computers. J. Geophys. Res. 102 (C3), 5753–5766.

McDougall, T.J., Jackett, D.R., Wright, D.G., Feistel, R., 2003. Accurate and computationally efficient algorithms for potential temperature and density of seawater. J. Atmos. Ocean. Technol. 20 (5), 730–741.

Mestres, M., Sierra, J.P., Sanchez-Arcilla, A., 2007. Factors influencing the spreading of a low–discharge river plume. Cont. Shelf Res. 27 (16), 2116–2134.

Murphy, P.L., Valle-Levinson, A., 2008. Tidal and residual circulation in the St. Andrew Bay system, Florida. Cont. Shelf Res. 28 (19), 2678–2688.

Murty, P.L.N., Sandhya, K.G., Bhaskaran, P.K., Jose, F., Gayathri, R., Balakrishnan Nair, T.M., Srinivasa Kumar, T., Shenoi, S.S.C., 2014. A coupled hydrodynamic modeling system for PHAILIN cyclone in the Bay of Bengal. Coast. Eng. 93, 71–81.

Nash, J.D., Moum, J.N., 2005. River plumes as a source of large–amplitude internal waves in the coastal ocean. Nature 437.

Osadchiev, A., 2015. A method for quantifying freshwater discharge rates from satellite observations and Lagrangian numerical modeling of river plumes. Environ. Res. Lett. 10.

Osadchiev, A., Sedakov, R., 2019. Spreading dynamics of small river plumes off the northeastern coast of the black sea observed by landsat 8 and sentinel-2. Remote Sens. Environ. 221, 522–533.

Osadchiev, A.A., Zavialov, P.O., 2013. Lagrangian model of a surface–advected river plume. Cont. Shelf Res. 58, 96–106.

Ou, S., Zhang, H., Wang, D., 2009. Dynamics of the buoyant plume off the Pearl River Estuary in summer. Environ. Fluid Mech. 9 (5), 471–492.

Pan, J., Gu, Y., Wang, D., 2014. Observations and numerical modeling of the Pearl River plume in summer season. J. Geophys. Res. Ocean. 119 (4), 2480–2500.

Passeri, D.L., Hagen, S., Bilskie, M., Medeiros, S.C., 2015. On the significance of incorporating shoreline changes for evaluating coastal hydrodynamics under sea level rise scenarios. Nat. Hazards 75 (2), 1599–1617.

Pinones, A., Valle-Levinson, A., Narvaez, D.A., Vargas, C.A., Navarrete, S.A., Yuras, G., Castilla, J.C., 2005. Wind-induced diurnal variability in river plume motion. Estuar. Coast. Shelf Sci. 65, 513–525.

Roth, M.K., 2016. Material Transport in the Inner Shelf of the Northern Gulf of Mexico (Ph. D. thesis). Naval Postgraduate School, Monterey, California.

Roth, M.K., MacMahan, J., Reniers, A., Ozgokomen, T.M., Woodall, K., Haus, B., 2017. Observations of inner shelf cross–shore surface material transport adjacent to a coastal inlet in the northern Gulf of Mexico. Cont. Shelf Res. 137, 142–153.

Shapiro, R., 1970. Smoothing, filtering, and boundary effects. Rev. Geophys. 8 (2), 359–387.

Shi, J.Z., Lu, L., Liu, Y., 2010. The hydrodynamics of an Idealized estuarine plume along a straight coast: A numerical study. Environ. Model. Assess. 15 (6), 487–502.

Sikiric, M.D., Janekovic, I., Kuzmic, M., 2009. A new approach to bathymetry smoothing in sigma–coordinate ocean models. Ocean Model. 29 (2), 128–136.

Stumpf, R.P., Gelfenbaum, G., Pennock, J.R., 1993. Wind and tidal forcing of a buoyant plume, Mobile Bay, Alabama. Cont. Shelf Res. 13 (11), 1281–1301.

Tarya, A., van der Vegt, M., Hoitink, A.J.F., 2015. Wind forcing controls on river plume spreading on a tropical continental shelf. J. Geophys. Res. Ocean. 120 (1), 16–35.

Taylor, J.R., 1997. An Introduction to Error Analysis: The Study of Uncertainties in Physical Measurement, second ed. University Science Books.

Taylor, K.E., 2011. Summarizing multiple aspects of model performance in a single diagram. J. Geophys. Res. 106, 7183–7192.

Towns, J., Cockerill, T., Dahan, M., Foster, I., Gaither, K., Grimshar, A., Hazlewood, V., Lathrop, S., Lifka, D., Peterson, G.D., Roskies, R., Scott, J.R., Wilkins-Diehr, N., 2014. XSEDE: Accelerating scientific discovery. Computing in Science & Engineering 16, 62–74.

UCF, 2011a. Digital Elevation Model and Finite Element Mesh Development. Tech. rep.. Northwest Florida Water Management District and the Federal Emergency Management Agency.

UCF, 2011b. Flood Insurance Study: Florida Panhandle and Alabama, Model Validation. Tech. rep.. Federal Emergency Management Agency.

Valle-Levinson, A., Huguenard, K., Ross, L., Branyon, J., MacMahan, J., Reniers, A., 2015. Tidal and nontidal exchange at a subtropical inlet: Destin Inlet, Northwest Florida. Estuar. Coast. Shelf Sci. 155, 137–147.
Walpole, R.E., Myers, R.H., Myers, S.L., Ye, K.E., 2012. Probability and Statistics for Engineers and Scientists, ninth ed. Pearson Prentice Hall.
Westerink, J.J., Luettich, Jr., R.A., Feyen, J.C., Atkinson, J.H., Dawson, C.N., Roberts, H.J., Powell, M.D., Dunion, J.P., Kubatko, E.J., Pourtaheri, H., 2008. A basin to channel scale unstructured grid hurricane storm surge model applied to southern louisiana. Mon. Weather Rev. 136, 833–864.
Whitney, M.M., Garvine, R.W., 2005. Wind influence on a coastal buoyant outflow. J. Geophys. Res. 110.
Wilkin, J.L., Hunter, E.J., 2013. An assessment of the skill of real–time models of mid–atlantic bight continental shelf circulation. J. Geophys. Res. Ocean. 118 (6), 2919–2933.
Xia, M., Xie, L., Pietrafesa, L.J., 2007. Modeling of the cape fear river estuary plume. Estuar. Coasts 30 (4), 698–709.
Xia, M., Xie, L., Pietrafesa, L.J., Whitney, M.M., 2011. The ideal response of a Gulf of Mexico estuary plume to wind forcing: Its connection with salt flux and a Lagrangian view. J. Geophys. Res. Ocean. 116 (C8).
Xing, J., Davies, A.M., 1999. The effect of wind direction and mixing upon the spreading of a buoyant plume in a non-tidal regime. Cont. Shelf Res. 19, 1437–1483.
Yu, X., Guo, X., Morimoto, A., Buranapratheprat, A., 2018. Simulation of river plume behaviors in a tropical region: Case study of the Upper Gulf of Thailand. Cont. Shelf Res. 153, 16–29.
Zhang, Y., Baptista, A.M., 2008. Selfe: A semi-implicit Eulerian–Lagrangian finite-element model for cross-scale ocean circulation. Ocean Model. 21, 71–96.
Zhao, J., Gong, W., Shen, J., 2018. The effect of wind on the dispersal of a tropical small river plume. Frontiers Earth Sci. 12 (1), 170–190.
Zheng, Q., Clemente-Colon, P., Yan, X., Liu, W.T., Huang, N.E., 2004. Satellite synthetic aperture radar detection of delaware Bay plumes: jet–like feature analysis. J. Geophys. Res. Ocean. 109 (C3).